Measuring Extreme Diffusion in Physical Systems

by

Aileen Carroll Godfrey

A dissertation accepted and approved in partial fulfillment of the
requirements for the degree of
Doctor of Philosophy
in Physics

Dissertation Committee:
Raghu Parthasarathy, Chair
Eric Corwin, Advisor & Core Member
Laura Jeanty, Core Member
Leif Karlstrom, Institutional Representative

University of Oregon
Spring 2025

© 2025 Aileen Carroll Godfrey
This work is openly licensed via
CC BY-NC-ND 4.0.



DISSERTATION ABSTRACT

Aileen Carroll Godfrey

Doctor of Philosophy in Physics

Title: Measuring Extreme Diffusion in Physical Systems

Diffusive processes have been studied intensively since the 17th and 18th centuries. Significant progress was made in the 20th century, when Einstein modelled diffusion as a process where each particle in a diffusive system takes random steps in random directions through time, undergoing an overall random walk. This model, connected to statistical and differential equation descriptions of physical systems, has worked incredibly well to describe the average diffusing particle. However, this model fails to accurately capture the behavior of the extreme particles, such as those farthest from the origin or those which travel a certain distance first. Other methods have the potential to better describe the extremes, such as a random walk where each step is given a bias that changes in space and time. The work presented here seeks to measure extremes in diffusion numerically and experimentally. We make numerical measurements of the furthest particle, revealing that information about the environment itself can be extracted from measurements of the variance of the extreme particle location. We design an experimental system that will allow us to measure extreme first passage times in colloid diffusion. Finally, we make first passage time measurements of photons, which reveal the failure of the underlying Einstein random walk behind typically used photon transport models and show the need for a better model to describe the behavior and capture the extremes.

This dissertation includes both previously published and unpublished co-authored material.

CURRICULUM VITAE

NAME OF AUTHOR: Aileen Carroll Godfrey

GRADUATE AND UNDERGRADUATE SCHOOLS ATTENDED:

University of Oregon, Eugene, OR, USA
Brigham Young University – Idaho, Rexburg, ID, USA

DEGREES AWARDED:

Doctor of Philosophy, Physics, Spring 2025, University of Oregon
Master of Science, Physics, Winter 2021, University of Oregon
Bachelor of Science, Physics - Geophysics Emphasis, Winter 2018, Brigham Young University - Idaho

AREAS OF SPECIAL INTEREST:

Soft condensed matter, wave propagation and scattering, geophysics

PROFESSIONAL EXPERIENCE:

Research Assistant/PhD Candidate, University of Oregon, 2019-2025
Research Fellow, Center for Space Nuclear Research, 2018
Founder & Team Lead, BYU-Idaho High Altitude Research Team, 2017-2018

PUBLICATIONS:

A.N. Carroll-Godfrey, E.I. Corwin, “Measurements of extreme first passage times in photon transport", *arXiv preprint*, arXiv:2502.19359 (2025).

J.B. Hass, A.N. Carroll-Godfrey, I. Corwin, E.I. Corwin, “Anomalous fluctuations of extremes in many-particle diffusion” , Vol. 107, Issue 2, pp. L022101. DOI: 10.1103/PhysRevE.107.L022101 (2023).

ACKNOWLEDGEMENTS

Gratitude for Ben, for being my support through every step. For my little research assistant Eleanor, who joined me in 2021. She makes it all worth it.

For my family, especially my dad, because I wouldn't have chosen to pursue physics without his encouragement. For friends, near and far, who helped me stay afloat through this series of unfortunate events.

Thanks to everyone who watched Ellie so I could fit in another hour or two of work. For Heather, Sky, Max, Maddy, and the other incredible teachers and staff at the Co-op Family Center who loved my child and helped her grow.

Heartfelt appreciation for everyone who got me coffee/a treat or told me about the free food in such-and-such building. For my labmates: Jacob Hass, Eddie Bautista, Viola Bolton-Lum, and Franscesca Ark (who holds the record for gifted treats, I am forever indebted). For my advisor Eric Corwin, committee chair Raghuveer Parthasarathy (and the laser I stole from his lab), various physics faculty who lent a listening ear and voices of support, and Markus Allgaier for helping me far more than some random postdoc in another lab needed to.

This work was supported by the W.M. Keck Foundation Science and Engineering grant on "Extreme Diffusion".

To Dad.

“Remember to enjoy what you are doing.

If life seems difficult, remember what makes you happy.”

DISCLAIMER

No generative “A.I.” was used in the making of this document or the work presented herein.

TABLE OF CONTENTS

Chapter Page

I. INTRODUCTION 14

II. ANOMALOUS FLUCTUATIONS OF EXTREMES IN MANY-PARTICLE DIFFUSION 21

2.1. Abstract 21

2.2. Introduction 21

2.3. Background 23

2.4. Models for diffusion 25

2.5. Numerical Methods 27

2.6. Asymptotic Theory Results 29

2.7. Comparison of Numerical and Theoretical Results 31

2.8. Conclusion 33

2.9. Acknowledgements 34

2.10. Supplementary Material 35

2.10.1. Numerical Methods 35

2.10.2. Asymptotic Theory Results 37

2.10.2.1. SSRW Max_t^N 37

2.10.2.2. RWRE Env_t^N 39

2.10.2.3. RWRE Sam_t^N and Max_t^N 43

III. MEASUREMENTS OF EXTREME FIRST PASSAGE TIMES IN COLLOID SUSPENSIONS 47

3.1. Introduction 47

3.2. Background 47

3.3. Experimental design 52

Chapter Page

3.4. Preliminary results 54

3.5. Conclusion 58

3.6. Supplementary Material 59

IV. MEASUREMENTS OF EXTREME FIRST PASSAGE TIMES IN PHOTON TRANSPORT 70

4.1. Abstract 70

4.2. Motivation 70

4.3. Introduction 72

4.4. Background 72

4.5. Experimental Methods 74

4.6. Models for Photon Transport 76

4.6.1. The equation of transfer 76

4.6.2. Diffusion approximation 77

4.6.3. Telegraph equation 78

4.7. Results and Discussion 80

4.8. Conclusion 81

4.9. Acknowledgments 81

V. CONCLUSION 82

LIST OF FIGURES

Figure Page

1.1. A particle undergoing a one dimensional random walk. The particle takes one "step" in a random direction after the other, through time. Red arrows indicate rightward movement, and blue arrows indicate leftward movement. 15

1.2. 1D visualization of the Einstein and Barraquand-Corwin models, where the red and blue colors indicate the direction of each bias - right and left, respectively - and the color intensity indicates the strength of the bias; for example, a dark red square indicates a strong bias to the right for the particles inhabiting that square. White squares have an equal bias in each direction. Time increases from the bottom of the image toward the top. 16

1.3. Einstein and Barraquand-Corwin diffusion models. Einstein's diffusion model has an equal bias in each direction, and the particles diffuse accordingly. For the Barraquand-Corwin model, the red and blue colors and color intensity indicate the direction and strength of the bias as in Figure 1.2. Time increases from the bottom of the image toward the top. There is a noticeable difference in how the outlier particles for each model spread in the same amount of time. 17

2.1. A system of $N = 10^5$ particles evolving in a given random environment. The heat map records the site occupancy density. We also plot in green the asymptotic theory mean location for the maximum particle location. Around this is a shaded region with a width of two standard deviations based on the asymptotic theory variance. This region generally contains the extreme-most particle over time. The zoomed-in inset shows the spatial locations of $N = 10^2$ particles over time. Color indicates the bias (red is biased down and blue is biased up) and is chosen independently at each space-time box. The location of particles within each box is chosen for ease of visualization. 23

2.2. Plots of $\mathrm{Var}^{\mathrm{num}}\left(\mathrm{Max}_t^N\right)$ (solid) computed over 10000, 5000, 1000, 500 and 500 environments (respectively) and $\mathrm{Var}^{\mathrm{asy}}\left(\mathrm{Max}_t^N\right)$ (dashed) for $N = 10^2, 10^7, 10^{24}, 10^{85}, 10^{300}$ 28

Figure Page

2.3. Plots of $\mathrm{Var}^{\mathrm{num}}\left(\mathrm{Env}_t^N\right)$ (transparent solid) computed over 500 environments, $\mathrm{Var}^{\mathrm{asy}}\left(\mathrm{Env}_t^N\right)$ (dashed), and $\mathrm{Var}^{\mathrm{num}}\left(\mathrm{Max}_t^N\right) - \mathrm{Var}^{\mathrm{asy}}\left(\mathrm{Sam}_t^N\right)$ (dark solid) smoothed in each $1/25^{th}$ of a decade for $N = 10^2, 10^7, 10^{24}, 10^{85}, 10^{300}$. The three curves agree as shown in the zoomed-in inset. 29

2.4. Variance of the maximal particle $\delta\mathrm{Max}_t^N$ (red), environment $\delta\mathrm{Env}_t^N$ (blue), and sampling $\delta\mathrm{Sam}_t^N$ (green) for RWRE, and variance of the maximal particle $\delta\mathrm{Max}_t^N$ (purple) for SSRW, all for $N = 10^7$. Dashed lines are $\mathrm{Var}^{\mathrm{asy}}(\bullet)$, while solid lines are $\mathrm{Var}^{\mathrm{num}}(\bullet)$. $\mathrm{Var}^{\mathrm{num}}\left(\mathrm{Max}_t^N\right) - \mathrm{Var}^{\mathrm{asy}}\left(\mathrm{Sam}_t^N\right)$ (orange; smoothed as in Fig. 2.3) closely matches the environment curve (blue). 32

2.5. The asymptotic mean functions $M_1(N,t)$ and $M_2(N,t)$ are plotted for $N = 10^{85}$ in red and blue dashed lines, respectively. They agree closely for the full range of $t > \log(N)$ and also match the numerically measured values $\mathrm{Mean}^{\mathrm{num}}\left(\mathrm{Max}_t^N\right)$ given by the purple curve (which is linear, as expected, until roughly time $t = \log(N)$). 43

2.6. The asymptotic variance functions $V_1(N,t)$ and $V_2(N,t)$ are plotted for $N = 10^{85}$ in red and blue dashed lines, and the stitched together formula for $\mathrm{Var}^{\mathrm{asy}}\left(\mathrm{Env}_t^N\right)$ from (2.19) is plotted as the black dashed line. The purple curve is the numerically measured curve $\mathrm{Var}^{\mathrm{num}}\left(\mathrm{Env}_t^N\right)$. The inset shows how the stitching captures the transition between the two asymptotic curves V_1 and V_2, and the solid lines show the asymptotic power-laws that V_1 and V_2 demonstrate as $t \to \infty$. The vertical dotted line indicates the regime crossover at $t = (\log(N))^2$. 44

2.7. The mean position of the maximal particle location (solid line) for $N = 10^2, 10^7, 10^{24}, 10^{85}$ and 10^{300} for 10000, 5000, 1000, 500 and 500 instantiations of the environment, respectively. The theoretical prediction (dashed line) given in Eq. (2.24) is also shown. We find the theoretical predictions for the mean position of the maximum particle, $\mathrm{Mean}\left(\mathrm{Max}_t^N\right)$, are in agreement with the data. 46

3.1. Predicted extreme first passage times for $d = 1.18\ \mu$m silica colloids suspended in water at room temperature diffusing across distances up to 5mm from the origin. EFPT predictions from the origin to a distance L of 5mm vary from around 10 days for a system of $N = 5 \times 10^9$ colloids (25% colloids by weight) to nearly 60 days for $N = 2 \times 10^2$ colloids. 49

Figure Page

3.2. Render of the experimental setup, using CAD designs. The centrifuge base plate, rotor plate, support arm, and braces were designed and machined specifically for use with the motor, rotary encoder, and tachometer. The rotor plate is designed with 16 channels of two depths, fabricated on a CNC mill for precision, allowing different capillary widths to rest securely in the plate. Circular holes allow light from the microscope to pass through the capillaries for imaging. While the capillaries may be up to 100mm long, only the first few millimeters from the outer edge can be imaged; see Figure 3.1, where such distances correspond to EFPTs on the order of multiple days or even weeks. The microscope shown is an approximate model of the Nikon Eclipse FN-1 used in this experiment, with a camera attached to the C-mount. 51

3.3. Examples of imaged capillary at start of time lapse and 300 frames later. Colloids enter from the top left corner, suggesting that the capillary was placed at a slight angle and that gravity is drawing colloids to the upper capillary wall. 55

3.4. Examples of edits that can be made to highlight features in images of capillaries. The left image has had the contrast increased, the center image has also been run through a bandpass filter, and the right image has additionally had the brightest pixels enhanced via the ImageJ Maximum filter. 56

3.5. Examples of an air bubble inside a capillary, and how it affects colloid centrifuging and diffusion. The left frame was captured immediately after centrifuging, and the right frame was taken approximately 50 hours later. 56

3.6. Other issues encountered include capillaries placed at an angle (left), servo positioning failures (center), and capillaries that are disturbed from the original placement and end up out of the microscope focus (right). 57

4.1. Experimental setup, consisting of elements described in the text. Signals are collected over an adjustable time period, resulting in a histogram of EFPTs. An example of such a histogram at three different concentrations of scattering media is shown, with concentration increasing from left to right, where the x axis is the time relative to the speed of light in a vacuum, and the y axis is the probability of that time as the EFPT. 73

Figure Page

4.2. EFPT differences measured experimentally, in picoseconds, versus volume concentration C. Both plots are the same, with different scales. Solid lines are predicted EFPTs for a photon traveling through an index-averaged medium of silica and water. Experimental values are shown as points, telegraph equation predictions are shown as dashed lines, and the diffusion approximation is shown as dotted lines. Color indicates wavelength from 680 nm (violet) to 830 nm (orange). Predictions were made using $N = 5 \times 10^6$ photons. The orange dotted line does not appear in this figure as the values fail to cross over the measured range. 79

CHAPTER I

INTRODUCTION

In *De Rerum Natura*, a first-century B.C. didactic poem, the Roman philosopher Lucretius postulates that dust particles floating about in a ray of sunlight are propelled by smaller, invisible collisions with their enviornment:

> "No doubt, this roaming motion in all particles comes from primordial elements of things, for by themselves these primary elements are moved, and then from that motion bodies in small compounds, those which are, as it were, closest to the force of primary matter, are set in motion by the impulses of blind collisions with those particles, and then they themselves stir compound bodies of slightly larger size. And thus, motion rises from basic particles and goes, little by little, up to our senses, so that those things we can see in sunlight are shifted, too, although we do not see the impacts that bring about their motion." [1]

This could be considered one of the earliest records of someone seeking to understand what we know today as diffusion, the general process by which a substance spreads out throughout time. When the European Scientific Revolution led to the Age of Enlightenment in the 17th century, the study of heat and its motion became a particularly "hot" topic [2–5]. As a result, in the 18th century, significant developments were made in understanding fluid mechanics and the kinetic theory of gases, as well as describing thermal conduction with similar frameworks [6–8]. With the birth of modern thermodynamics in the 19th century, scientists continued to make strides in understanding the motion of both heat and particles, from steam engines to fluids in motion [9–14]. Of particular note were the Boltzmann transport equation, which characterized out-of-equilibrium thermodynamic systems through statistical quantities [15], and the

Navier-Stokes continuum equations for fluid transport [16, 17]. Experimental work during this time also contributed to the understanding of diffusive processes – Thomas Graham studied gas diffusion [18] and Adolph Fick measured concentrations of salt in water, leading to the influential differential equations now referred to as Fick's laws of diffusion [19].

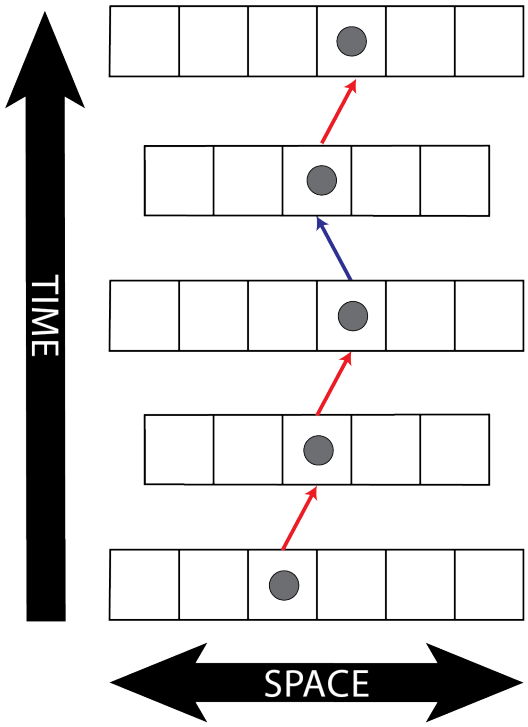


Figure 1.1. A particle undergoing a one dimensional random walk. The particle takes one "step" in a random direction after the other, through time. Red arrows indicate rightward movement, and blue arrows indicate leftward movement.

The first known observations of irregular, wiggly movements characteristic of small particles may be attributed to the work of Jan Ingenhousz, who described the motion of coal dust on the surface of alcohol in 1785 [20]. In the following century, while scientists worked to develop theoretical frameworks and mathematical models to describe the mechanisms for how gases, liquids, particles, and heat disperse, Robert Brown published observations of the seemingly random motion of diffusive particles such

as the dust that floats through air and the motion of pollen on the surface of water [21–23]. Brown's descriptions of this motion became quite prolific, and the name "Brownian motion" caught on. The connection between diffusion models and Brownian motion observations was built on the concept of the "random walk", proposed in Jules Regnault's 1863 publication and later developed in Louis Bachelier's 1900 thesis. Both works described small price changes in stock market shares as random and unpredictable "steps" within an overall "walk" [24, 25]. In 1905, Einstein used a random walk model to formulate a diffusion equation to describe Brownian motion, with a diffusion coefficient controlling the size of the diffusing particles' steps [26]. Marian von Smoluchowski and William Sutherland both independently, concurrently characterized Brownian motion using the same theoretical framework [27, 28].

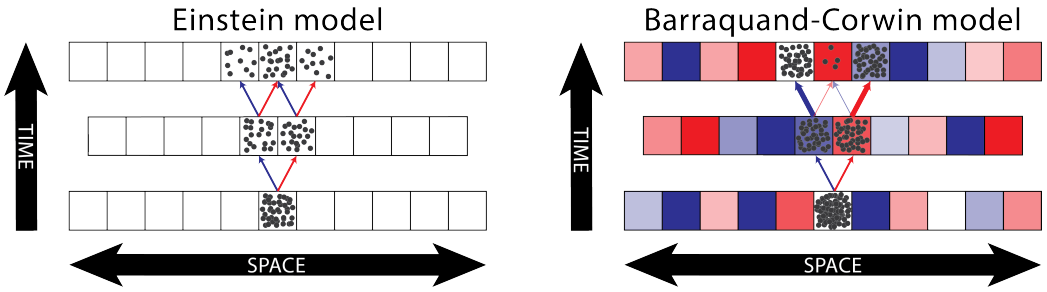


Figure 1.2. 1D visualization of the Einstein and Barraquand-Corwin models, where the red and blue colors indicate the direction of each bias - right and left, respectively - and the color intensity indicates the strength of the bias; for example, a dark red square indicates a strong bias to the right for the particles inhabiting that square. White squares have an equal bias in each direction. Time increases from the bottom of the image toward the top.

The random walk model for diffusion proposed that the visible particles undergoing Brownian motion move through an invisible environment of constantly moving molecules, which are driven by their inherent thermal energy. These molecules collide with the larger visible particles from all sides, causing the apparent erratic motion. These collisions with the environment cause the diffusing particles to undergo a random

walk with independent random "steps" that change their location throughout time. An example of a single particle undergoing a random walk is shown in Figure 1.1, where the particle has an equal probability of stepping to the right or the left at every moment in time. The distribution of particle steps has a variance governed by a diffusion coefficient, which depends on the properties of the diffusing particle, including its size and density, and the surrounding environment, such as its density and viscosity. Einstein derived the Brownian motion random walk model through the molecular-kinetic theory of heat, linking it to Fick's earlier differential diffusion equation and expressing the diffusion coefficient in terms of statistical properties and these measurable physical quantities [26]. Experimentalists Jean Baptiste Perrin and Christina Cruickshank Miller confirmed the validity of Einstein's, Sutherland's, and Smoluchowski's work [29, 30].

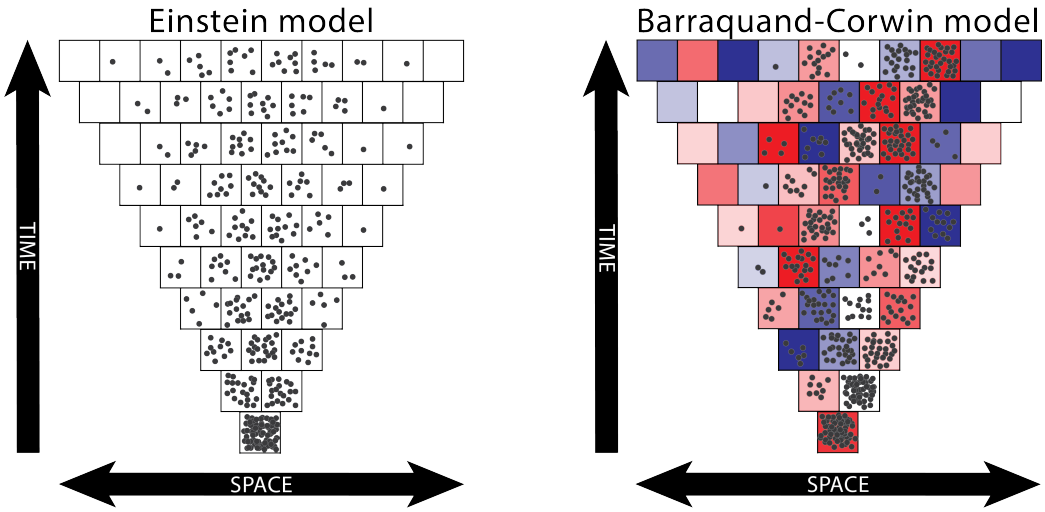


Figure 1.3. Einstein and Barraquand-Corwin diffusion models. Einstein's diffusion model has an equal bias in each direction, and the particles diffuse accordingly. For the Barraquand-Corwin model, the red and blue colors and color intensity indicate the direction and strength of the bias as in Figure 1.2. Time increases from the bottom of the image toward the top. There is a noticeable difference in how the outlier particles for each model spread in the same amount of time.

The random walk model's results, from the diffusion differential equation to the Stokes-Einstein-Sutherland relation, can be used to understand many processes dominated

by diffusion of the bulk of the material. The ability to describe the average diffusing particle and predict statistical behavior has led to advances in applications, including a broad range of human biological and chemical processes [31–38] as well as genetics [39–42]. However, while the random walk model of diffusion effectively describes average particle behavior, it fails in many situations, such as when active matter injects energy into the system [43, 44], when Levy flights or other anomalous diffusion processes better describe the dynamics [45–48], or when the diffusion coefficient varies in space or time [49]. Some applications require the addition of new concepts to the foundational "Einstein" random walk, such as a random walk in fractal media [50, 51] or a random environment [52, 53]. Model failures are especially noticeable with outlier or extreme particles, the particles that are located the farthest from the origin or which cross a given distance first, and these extreme particles are critical in many applications that rely on the first particle to travel from the origin to a specific distance or target, including stock market fluctuations [54, 55] chemical reactions and channel transport [56, 57], fertilization [58, 59], protein dynamics [60] and menopause timing [61].

The Einstein random walk assumes that each particle follows a completely independent path, unaffected by nearby particles and their motion, even though we would expect neighboring particles to be influenced in similar ways by their shared environment. To account for background correlations, one could instead require that particles undergo a random walk in a random environment, where the probability that a particle will "step" in a given direction varies in space and time. Such an environment can be seen in Figure 1.2, contrasted with that of the "Einstein" uncorrelated random walk. By replacing the equal probability that a particle will move right or left with a biased probability that changes in space and time, we can portray the correlated environment in a way that allows neighboring particles to be influenced in the same way. As seen in Figure 1.3,

while average particle behavior remains essentially the same between the models, the behavior of the outlier particles varies. Particle motion in the correlated environment is more "sticky": particles close to each other remain together, following the environmental biases. In particular, we expect the outlier particles to be characterized by different statistics than the average [62–64], and we anticipate the emergence of different scaling regimes depending on system size as well as length and time scales [52, 53].

Additionally, light sent into random media scatters in a way that appears analogous to random-walk-model diffusion. With relatively high scatterer concentration and minimal absorption, we can use a diffusion approximation to the nontrivial Boltzmann Radiative Transfer Equation to model photon transport [65, 66]. The diffusion approximation predicts the behavior of the average photon travelling through random media well, and offers valuable insights into systems in many applications [66–72]. However, this approximation neglects the speed of light in a medium, and as a result, has significant limitations [73–75]. By retaining a second-order time derivative in the diffusion approximation, or by accounting for photons as two opposing "streams", we can find a telegraph equation model that factors in this constant speed of light and overcomes many of the diffusion approximation limitations [76, 77]. A telegraph equation model overcomes many of the diffusion approximation limitations by accounting for ballistic photons and wave-like effects present at small distances, leading to more accurate predictions of photon behaviors [49, 76–82]. Both models have described the average photon well, and photon propagation in scattering media has been characterized and used in a broad range of applications [65, 66, 69–71, 77, 81]. However, the extreme value statistics of photons in scattering media have not been measured, and could reveal the limits of the uncorrelated random walk model that underlies both of these approximations to the radiative transfer equation.

The following chapters are a coauthored paper, unpublished work, and a first author paper, all of which I composed during my time as a graduate student. Chapter II (co-authored work, published in PRE [83]) explores a method developed with Eric Corwin and Jacob Hass. We numerically simulated diffusive systems in a Beta-distributed biased environment and measured the location of the farthest particle from the origin. In doing so, we uncovered a new phase with connections to the Kardar-Parisi-Zhang universality class. In chapter III, I developed an experimental apparatus that doubles as a centrifuge and a microscope stage in order to observe diffusion in colloidal suspensions. I report on current design and the potential for future work, particularly in verification of results from Chapter II and additional work by Hass et al on extreme first passage times [84]. In Chapter IV (co-authored work, in review, [85]), I used an ultrafast pulsed laser and time-correlated single photon counting to send bursts of photons into a tube filled with silica nanospheres, time the first photon to exit the tube, and build histograms of extreme first passage times. I measured the peak of this distribution, and determined that neither the diffusion nor telegraph model for photon transport correctly predicts the peak location; correlations cause more photons to travel directly through the tube as though they see an index-averaged medium.

CHAPTER II

ANOMALOUS FLUCTUATIONS OF EXTREMES IN MANY-PARTICLE DIFFUSION

2.1 Abstract

In many-particle diffusions, particles that move the furthest and fastest can play an outsized role in physical phenomena. A theoretical understanding of the behavior of such extreme particles is nascent. A classical model, in the spirit of Einstein's treatment of single-particle diffusion, has each particle taking independent homogeneous random walks. This, however, neglects the fact that all particles diffuse in a common and often inhomogeneous environment that can affect their motion. A more sophisticated model treats this common environment as a space-time random biasing field which influences each particle's independent motion. While the bulk (or typical particle) behavior of these two models has been found to match to high degree, recent theoretical work of Barraquand, Corwin and Le Doussal on a one-dimensional exactly solvable version of this random environment model suggests that the extreme behavior is quite different between the two models. We transform these asymptotic (in system size and time) results into physically applicable predictions. Using high precision numerical simulations we reconcile different asymptotic phases in a manner that matches numerics down to realistic system sizes, amenable to experimental confirmation. We characterize the behavior of extreme diffusion in the random environment model by the presence of a new phase with anomalous fluctuations related to the Kardar-Parisi-Zhang universality class and equation.

2.2 Introduction

Our world is fueled by outliers. Information in signals is carried by the leading edge [45, 57, 86–91]. A viral or bacterial infection is spread by the first few pathogens to enter a host and the first host to enter a new region [31, 92]. A species is evolved by the fittest mutations [41, 42, 93]. Scientific revolution is sparked by the first new idea. In all

of these contexts the precipitating action is driven by the extremes among a great number of agents (varying from $N \sim 10^2$ to $N \sim 10^{60}$ depending on the context) evolving in a complex but shared environment. How does the nature of the shared environment affect these outlier behaviors? Conversely, can we infer the nature of the shared environment from the behavior of these outliers? Despite their obvious importance, these overarching questions are still unanswered.

The classical model for many-particle diffusion as independent homogeneous random walks provides an easily calculable solution, but entirely neglects the effects of the shared and likely inhomogeneous environment. This model is the basis for diffusion coefficients [26, 94, 95], which succinctly describe the behavior of typical particles in a many-particle diffusion. A more sophisticated model treats the shared environment as a space-time random biasing field with short-range space-time correlations. Each particle thus articulates independent random walks subject to forcing by the common biasing field. While this refined model does not affect typical particle diffusion behavior [96], it drastically impacts the behavior of extreme particles. In this work, we provide predictions for the behavior of extreme particles moving in a random and inhomogenous environment. We find that the variance in the position of the extreme particle is a robust and sensitive measurement of the nature of the environment and show how this variance can be understood as the sum of two contributions: the randomness present in the environment, and the sampling of random walks in that environment. We show that by subtracting out the variance due to sampling we can produce direct measurements of the environment, inaccessible from measurements of the motion of a typical particle or of the bulk. This residual environmental variance is characterized by a novel power law that we demonstrate holds even when the number of particles is as small as a few hundred.

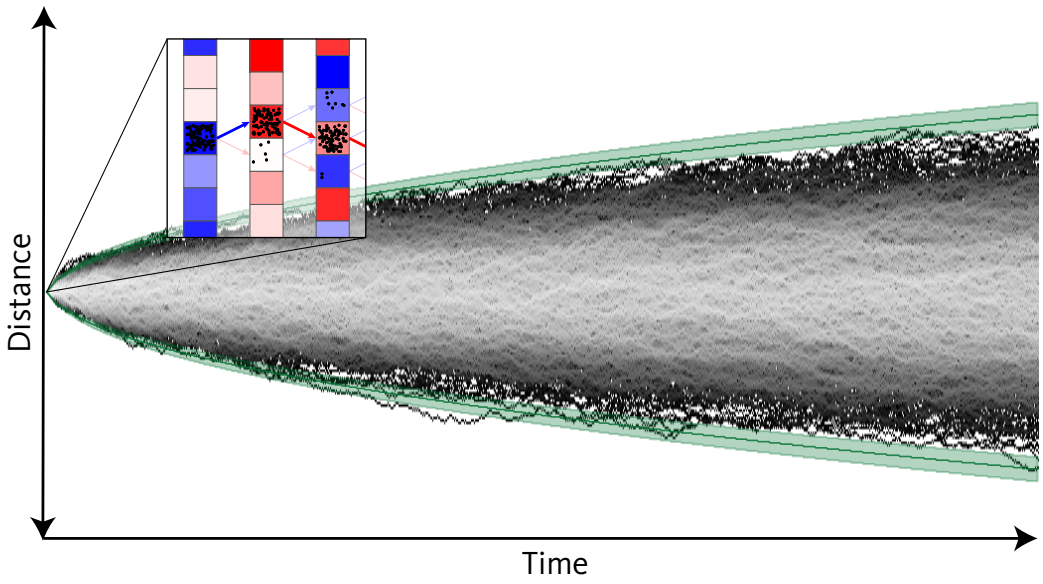


Figure 2.1. A system of $N = 10^5$ particles evolving in a given random environment. The heat map records the site occupancy density. We also plot in green the asymptotic theory mean location for the maximum particle location. Around this is a shaded region with a width of two standard deviations based on the asymptotic theory variance. This region generally contains the extreme-most particle over time. The zoomed-in inset shows the spatial locations of $N = 10^2$ particles over time. Color indicates the bias (red is biased down and blue is biased up) and is chosen independently at each space-time box. The location of particles within each box is chosen for ease of visualization.

2.3 Background

Building on observations by Brown [21, 22] from 1827, Einstein [26, 94, 95] (along with Langevin [97], Sutherland [27, 98] and Smoluchowski [28, 99]) proposed a theory of diffusion based on modeling particles by independent random walks with variance controlled by a diffusion coefficient intrinsic to the particle/environment pair. Soon after, Perrin experimentally verified Einstein's statistical predictions [29, 100].

Probing the effectiveness and limitations of Einstein's diffusion model has remained a challenge. On short time scales, particle motion is ballistic, dominated by inertia [101–106]. Many physically relevant situations require the addition of new concepts to accurately model them. Certain diffusive processes are better modeled

by Levy flights [46] or other types of anomalous diffusions [47, 48] instead of simple random walks. Other work has focused on active particles which inject energy into their environment [43, 44]. Further, in environments which are slowly mixing, Einstein's theory may also break down due to the presence of quenched disorder [46, 107]. Unlike the above deviations from the classical model, our approach is intended to describe generic many-particle diffusions.

The random walk in random environment (RWRE) model goes back to [108, 109] (see also [110–114]) and comes in two types – long-range [47, 115–119] and short-range [50, 120–125] temporally correlated environments. We focus here on the latter. In this context, typical RWRE particles behave like Brownian motion, matching the behavior from Einstein's model [126, 127]. The motion of atypical particles is controlled by large deviations of the RWRE's transition probability as first studied in [128].

Barraquand and Corwin [52] discovered the exactly solvable Beta RWRE discussed extensively below and uncovered a remarkable connection between its large deviations for times of order $\log(N)$ and the statistics of the Kardar-Parisi-Zhang (KPZ) universality class [129, 130], namely the Gaussian Unitary Ensemble (GUE) Tracy-Widom distribution [131]. Soon after [53] recognized that a phase transition should occur in the $(\log(N))^2$ time frame while [132] discovered that in this frame the GUE Tracy-Widom distribution is replaced by the KPZ equation one-point distribution [133–137]. See [138–144] for further developments. The recursion relation (2.3) for RWRE transition probabilities solves a discrete version of the multiplicative noise stochastic heat equation (mSHE)

$$\partial_t Z(x,t) = \frac{1}{2}\partial_x^2 Z(x,t) + \xi(x,t)Z(x,t) \tag{2.1}$$

with ξ space-time white noise. The logarithm of the mSHE $h(x,t) = \log Z(x,t)$ solves the KPZ equation

$$\partial_t h(x,t) = \frac{1}{2}\partial_x^2 h(x,t) + \frac{1}{2}(\partial_x h(x,t))^2 + \xi(x,t). \tag{2.2}$$

Hence, large deviations for RWREs, in particular beyond the solvable model and even in experimental settings, may relate to the KPZ equation and its universality class – especially in light of the rich canon of work on KPZ universality in various contexts using theoretical [129, 145], numerical [146, 147], and experimental [148] methods. The KPZ connection is quite useful since its statistics and power-laws are well studied.

2.4 Models for diffusion

Although physical diffusion is continuous in time and (typically) occurs in three-dimensional space, here we work with discrete models in one spatial dimension. The principal reason for this choice is that it is the setting for the exactly solvable Beta RWRE [52] (a continuous *sticky Brownian motion* limit of this model exists [140]) that will enable us to compare numerical results to exact theoretical predictions. Beyond that, discretization is common for numerical simulations and higher dimensions are more challenging numerically due to anisotropy issues arising from the choice of lattice and due to the lack of exactly solvable models, c.f. [53]. In real diffusion in a common environment, there will be length and time scales on which the environment decorrelates. Our discrete model can be thought of as coarse-graining the environment in space and time onto a lattice and thus we do not expect discrete and continuous models to differ greatly for long-times and large-scales. Our model ignores any higher order interactions as we expect them to be less present in the behavior of extreme particles, for which the local density is necessarily low. Additionally, there are physical settings where particles take discrete states [39, 149] or evolve in quasi-one-dimensional spaces [150, 151].

We study the *Beta RWRE* introduced in [52] (see Fig. 2.1). We model the environment by a collection $\mathbf{B} = \{B(x,t) : x \in \mathbb{Z}, t \in \mathbb{Z}_{\geq 0}\}$ of independent identically distributed random variables all drawn from the uniform distribution on $[0,1]$. At time $t = 0$ we start with N particles all at site 0. Given an instance of the environment $\mathbf{B}$ the particles proceed as follows. Each particle at x and t independently flips the same weighted coin which has probability $B(x,t)$ of heads (moving the particle to site $x+1$ at time $t+1$) and $1-B(x,t)$ of tails (moving to $x-1$ instead). Thus, while particles do not interact with each other, those at the same place and time are all influenced by the common environment.

This model is exactly solvable when $B(x,t)$ are distributed according to the Beta distribution, $Beta(\alpha,\beta)$ [52]. For simplicity, we focus on the special case $\alpha = \beta = 1$ corresponding to the uniform distribution. The classical simple symmetric random walk (SSRW) model arises in the limit $\alpha = \beta \to \infty$ where all $B(x,t) \equiv 1/2$ and the environment is deterministic.

We focus on the behavior of the right-most particle at time t. We denote this by Max_t^N, with N the number of particles in the system. Two types of randomness affect Max_t^N: that of the environment and that of sampling the random walks in that environment. The effect of the environment is via the transition probability $p_{\mathbf{B}}(x,t)$, the probability that a single random walker initially at 0 will end up at x at time t for a given environment $\mathbf{B}$. This satisfies the recursion relationship,

$$\begin{aligned} p_{\mathbf{B}}(x,t) =& p_{\mathbf{B}}(x-1,t-1)B(x-1,t-1) + \\ & p_{\mathbf{B}}(x+1,t-1)\big(1-B(x+1,t-1)\big) \end{aligned} \tag{2.3}$$

with initial condition $p_{\mathbf{B}}(0,0) = 1$ and $p_{\mathbf{B}}(x \neq 0,0) = 0$. Since each random walker is independent, conditional on the environment, the distribution of the ensemble of N walks is determined by $p_{\mathbf{B}}(x,t)$. Given the environment $\mathbf{B}$, the probability that a single random

walker is at or above x at time t is given by the tail probability, $P_{\mathbf{B}}(x,t) = \sum_{y \geq x} p_{\mathbf{B}}(y,t)$. This and the independence of random walkers, conditional on the environment, imply

$$\text{Prob}_{\mathbf{B}}(\text{Max}_t^N \leq x) = \big(1 - P_{\mathbf{B}}(x,t)\big)^N, \tag{2.4}$$

where the left-hand side is the probability, given the environment $\mathbf{B}$, that $\text{Max}_t^N \leq x$.

We study how Max_t^N varies upon sampling a new environment and random walkers therein. Eq. (2.4) suggests that a good proxy for Max_t^N is the location Env_t^N of the $1/N$-quantile of $P_{\mathbf{B}}(x,t)$, i.e., Env_t^N equals the maximal x such that $P_{\mathbf{B}}(x,t) > 1/N$. Notice that Env_t^N only accounts for the variation due to the environment. The variation due to sampling in that environment is denoted Sam_t^N and defined by $\text{Max}_t^N = \text{Env}_t^N + \text{Sam}_t^N$. We use the notation $\text{Mean}(\bullet)$ and $\delta\bullet$ for the mean and variance of a quantity $\bullet$ (e.g. $\text{Max}_t^N, \text{Env}_t^N, \text{Sam}_t^N$) averaged over both the environment and the sampling of random walkers in that environment.

2.5 Numerical Methods

We numerically simulate our models for system sizes varying from $N = 10^2$ to $N = 10^{300}$. We consider such large and physically unrealistic system sizes like 10^{300} in order to see how asymptotic theory applies for as wide a range as possible of finite system sizes. We evolve the system for times from $t = 0$ to $t = 5000\log(N)$. As explained below, $\log(N)$ and $(\log(N))^2$ set key timescales and our range of times ensure that for all choices of N, we encompass these scales. We simulate such large systems by tracking occupation variables instead of individual particle trajectories. In particular, if there are $N(x,t)$ particles at site x at time t, then the number that move to site $x+1$ is binomially distributed with $N(x,t)$ samples and success probability $B(x,t)$ (the remainder move to site $x-1$). We sample these binomial distributions utilizing quadruple-precision floating point numbers and making approximations to the binomial distribution when dealing with sizes beyond our precision limits, as described in Section 2.10. The rightmost particle

location (identified by the maximal x with $N(x,t) \geq 1$) at each time represents a sample of Max_t^N. By repeatedly sampling new environments along with random walk occupation variables $N(x,t)$ therein we numerically measure δMax_t^N. To distinguish from the true value we denote this numerically measured variance by $\text{Var}^{\text{num}}\left(\text{Max}_t^N\right)$ and plot it in Fig. 2.2. In like fashion, we measure $\text{Var}^{\text{num}}\left(\text{Env}_t^N\right)$ for each sampled environment by using Eq. 2.3 to compute $p_{\mathbf{B}}(x,t)$. Fig. 2.3 shows $\text{Var}^{\text{num}}\left(\text{Env}_t^N\right)$ as a function of time (see Section 2.10 for $\text{Mean}^{\text{num}}\left(\text{Max}_t^N\right)$ and $\text{Mean}^{\text{num}}\left(\text{Env}_t^N\right)$). The data presented in Fig. 2.2 and 2.3 took approximately three weeks to run in parallel on 500 cores of the University of Oregon high performance computing cluster, Talapas.

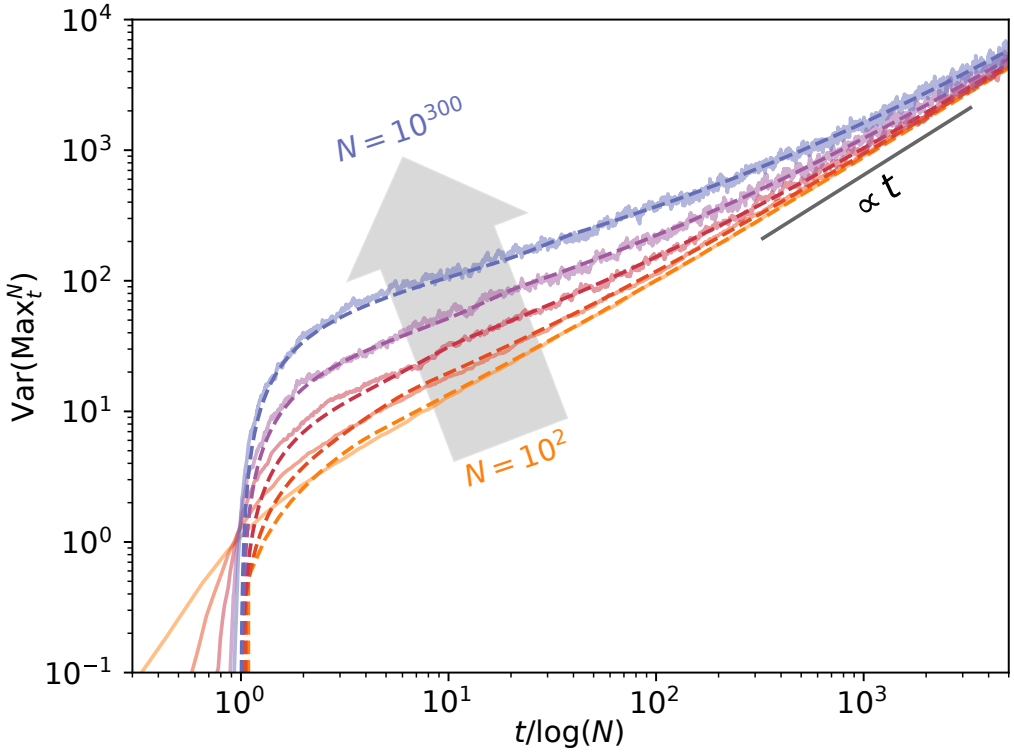


Figure 2.2. Plots of $\text{Var}^{\text{num}}\left(\text{Max}_t^N\right)$ (solid) computed over 10000, 5000, 1000, 500 and 500 environments (respectively) and $\text{Var}^{\text{asy}}\left(\text{Max}_t^N\right)$ (dashed) for $N = 10^2, 10^7, 10^{24}, 10^{85}, 10^{300}$

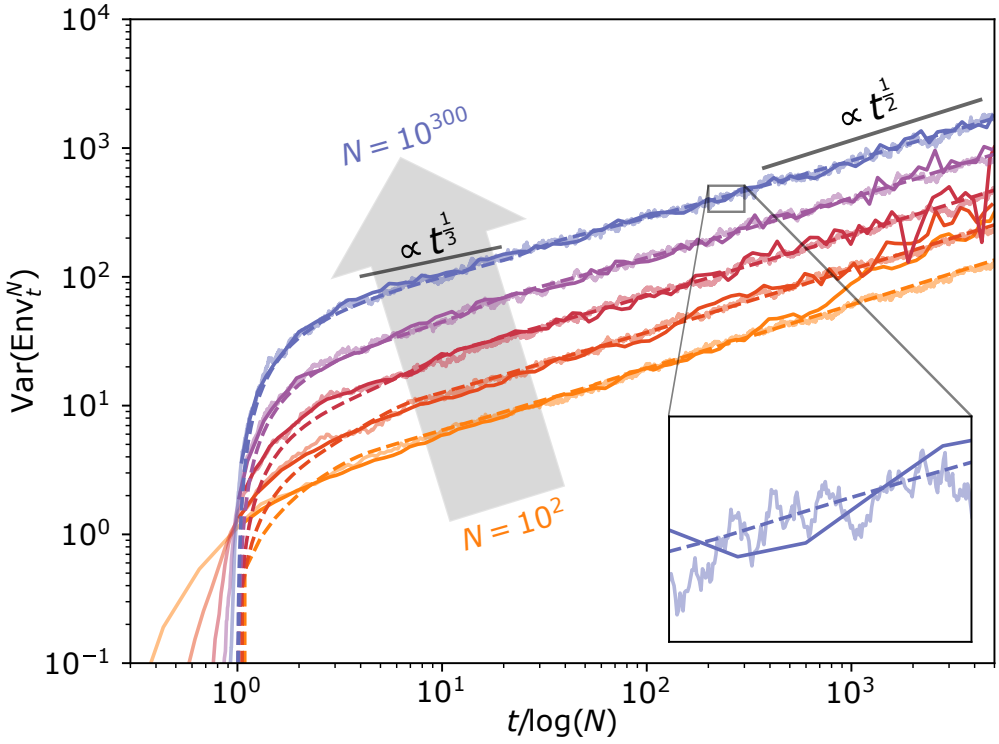


Figure 2.3. Plots of $\mathrm{Var}^{\mathrm{num}}\left(\mathrm{Env}_t^N\right)$ (transparent solid) computed over 500 environments, $\mathrm{Var}^{\mathrm{asy}}\left(\mathrm{Env}_t^N\right)$ (dashed), and $\mathrm{Var}^{\mathrm{num}}\left(\mathrm{Max}_t^N\right) - \mathrm{Var}^{\mathrm{asy}}\left(\mathrm{Sam}_t^N\right)$ (dark solid) smoothed in each $1/25^{th}$ of a decade for $N = 10^2, 10^7, 10^{24}, 10^{85}, 10^{300}$. The three curves agree as shown in the zoomed-in inset.

2.6 Asymptotic Theory Results

We describe asymptotic results on the behavior of Max_t^N, Env_t^N and Sam_t^N as both N and t tend to infinity in different limits. Given a fixed relationship between t and $\log(N)$ such as $t/\log(N) = \hat{t}$ or $t/\log(N)^2 = \hat{\hat{t}}$ for $\hat{t}$ or $\hat{\hat{t}}$ fixed, we write $f(N,t) \gg g(N,t)$ if $f(N,t)/g(N,t)$ tends to infinity as N and t do subject to their relationship. We use the notation $\mathrm{Var}^{\mathrm{asy}}(\bullet)$ to denote the asymptotic theory formula for the variance of $\bullet$, interpolated back to finite N and t. SSRW theory follows from Stirling's formula while asymptotic results for the RWRE rely on tools from quantum integrable systems [52, 132, 144] and are derived first for Env_t^N and then for Max_t^N and Sam_t^N.

SSRW Max_t^N**:** For $t/\log(N) = \hat{t}$ with fixed $\hat{t} < (\log 2)^{-1}$, we have $N \gg 2^t$ and hence with very high probability every reachable site in the lattice at time t is occupied, hence $\delta\mathrm{Max}_t^N \approx 0$. When $\hat{t} > (\log 2)^{-1}$, we show in Section 2.10 that Max_t^N is asymptotically a Gumbel random variable. For $\hat{t}$ large, $\mathrm{Var}^{\mathrm{asy}}\big(\mathrm{Max}_t^N\big) \approx \frac{\pi^2}{12}\frac{t}{\log(N)}$.

RWRE Env_t^N**:** For $t/\log(N) = \hat{t}$ with fixed $\hat{t} < 1$, $\delta\mathrm{Env}_t^N \approx 0$. To see this, note that $P_{\mathbf{B}}(t,t) = B_{0,0}\cdots B_{t-1,t-1}$. Taking logs and applying the central limit theorem shows that $\log\big(P_{\mathbf{B}}(t,t)\big) \approx -t + t^{1/2}G$ for G a standard Gaussian. This implies that $P_{\mathbf{B}}(t,t) \approx e^{-t} \gg 1/N$. Thus the RWRE stops saturating the lattice when $t = \log(N)$ plus a order $(\log(N))^{1/2}$ Gaussian fluctuation. For the SSRW this happens at time $\log_2(N)$ plus order one fluctuations.

$\delta\mathrm{Env}_t^N$ displays two asymptotic regimes. For fixed $t/\log(N) = \hat{t} > 1$, $\delta\mathrm{Env}_t^N$ takes asymptotic form,

$$V_1(N,t) := \Big(\frac{\log(N)}{t}\Big)^{2/3}\sigma_\chi^2\frac{2^{2/3}\big(1-\frac{\log(N)}{t}\big)^{4/3}}{1-\big(1-\frac{\log(N)}{t}\big)^2}, \tag{2.5}$$

where $\sigma_\chi^2 \approx 0.813$ is the variance of the GUE Tracy-Widom distribution [131, 152]. As shown in Section 2.10, this follows from the result of [52]: For $v \in (0,1)$, $\log P_{\mathbf{B}}(vt,t) = -tI(v) + t^{1/3}\sigma(v)\chi_t$ where $I(v) = 1-\sqrt{1-v^2}$, $\sigma(v) = (2I(v)^2/(1-I(v)))^{1/3}$ and χ_t is random converging to the GUE Tracy-Widom distribution as t goes to infinity.

For $t/(\log(N))^2 = \hat{\hat{t}}$, $\delta\mathrm{Env}_t^N$ takes asymptotic form

$$V_2(N,t) := \frac{t}{2\log(N)}\cdot\delta h\Big(0,\frac{4(\log(N))^2}{t}\Big), \tag{2.6}$$

where $h(0,s)$ is the height at 0 and time s of the *narrow wedge* solution to the KPZ equation (2.2). As shown in Section 2.10, this follows from [132]: For $v \in (0,\infty)$, $\log P_{\mathbf{B}}(vt^{3/4},t) \approx -\frac{v^2t^{1/2}}{2} - \log(t)/4 + \log(v) - v^4/12 + h(0,v^4)$.

Interpolating between these regimes, and extrapolating past $(\log(N))^2$ (see also [144]) we find two power-laws,

$$\mathrm{Var}^{\mathrm{asy}}\left(\mathrm{Env}_t^N\right) \approx \begin{cases} \sigma_\chi^2 \left(\frac{\log(N)}{2}\right)^{\frac{1}{3}} t^{\frac{1}{3}} & 1 \ll \frac{t}{\log(N)} \ll \log(N), \\ \frac{1}{2}\pi^{\frac{1}{2}} t^{\frac{1}{2}} & \frac{t}{\log(N)} \gg \log(N). \end{cases} \tag{2.7}$$

For finite N and t these regimes have a gentle crossover that we capture by setting $\mathrm{Var}^{\mathrm{asy}}\left(\mathrm{Env}_t^N\right) := I(N,t)V_1(N,t) + \left(1 - I(N,t)\right)V_2(N,t)$ where $I(N,t) := \frac{1}{2} \cdot \left(1 - \mathrm{erf}\left(\frac{t-(\log(N))^{3/2}}{(\log(N))^{4/3}}\right)\right)$ (with $\mathrm{erf}(x) = 2/\sqrt{\pi}\int_0^x e^{-t^2}dt$ the error function) interpolates from 1 to 0 over an interval of width $(\log(N))^{4/3}$ around $(\log(N))^{3/2}$.

RWRE Sam_t^N and Max_t^N: We identify the additional contribution from sampling the many-particle diffusion given an environment. Using Eq. (2.4) and Taylor expansion of the results of [52] and [132] quoted above, Section 2.10 shows that for $t/\log(N) = \hat{t} > 1$ the sample fluctuation Sam_t^N is of Gumbel type with variance

$$\mathrm{Var}^{\mathrm{asy}}\left(\mathrm{Sam}_t^N\right) = \frac{\pi^2}{6}\frac{\left(\frac{t}{\log(N)} - 1\right)^2}{2\frac{t}{\log(N)} - 1} \approx \frac{\pi^2}{12}\frac{t}{\log(N)} \tag{2.8}$$

as $\hat{t}$ grows. This limit matches the behavior of the SSRW model. In Section 2.10 we also show that Sam_t^N is asymptotically independent of Env_t^N, thus

$$\delta\mathrm{Max}_t^N \approx \delta\mathrm{Env}_t^N + \delta\mathrm{Sam}_t^N. \tag{2.9}$$

2.7 Comparison of Numerical and Theoretical Results

Fig. 2.2 and 2.3 show that the asymptotic theoretical predictions for $\delta\mathrm{Max}_t^N$ and $\delta\mathrm{Env}_t^N$ are in excellent agreement with the numerical measurements. Fig. 2.3 further shows that we reliably recover $\delta\mathrm{Env}_t^N$ using $\mathrm{Var}^{\mathrm{num}}\left(\mathrm{Max}_t^N\right) - \mathrm{Var}^{\mathrm{asy}}\left(\mathrm{Sam}_t^N\right)$, as expected from Eq. 2.9. Notably, while these results were derived for asymptotically large $\log(N)$ and t, they hold nearly perfectly down to $N = 10^2$. Fig. 2.3 reveals that while we readily see the long-time $t^{1/2}$ power-law for $\delta\mathrm{Env}_t^N$ from Eq. 2.7, the $t^{1/3}$ power-law is elusive. Although the full characterization of the short-time regime is in excellent

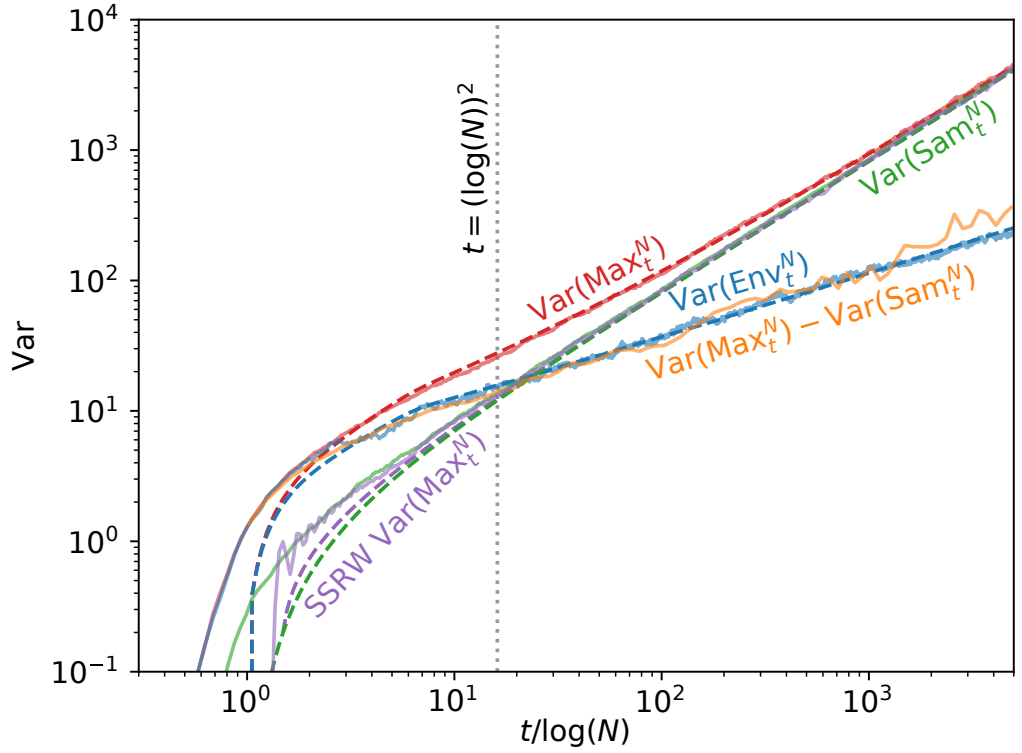


Figure 2.4. Variance of the maximal particle $\delta\mathrm{Max}_t^N$ (red), environment $\delta\mathrm{Env}_t^N$ (blue), and sampling $\delta\mathrm{Sam}_t^N$ (green) for RWRE, and variance of the maximal particle $\delta\mathrm{Max}_t^N$ (purple) for SSRW, all for $N = 10^7$. Dashed lines are $\mathrm{Var}^{\mathrm{asy}}(\bullet)$, while solid lines are $\mathrm{Var}^{\mathrm{num}}(\bullet)$. $\mathrm{Var}^{\mathrm{num}}\left(\mathrm{Max}_t^N\right) - \mathrm{Var}^{\mathrm{asy}}\left(\mathrm{Sam}_t^N\right)$ (orange; smoothed as in Fig. 2.3) closely matches the environment curve (blue).

agreement with the numerical results, the $t^{1/3}$ power-law is difficult to capture since the transitional window of $\log(N)$ to $(\log(N))^2$ is too narrow for realistic sizes of N, even up to $N = 10^{300}$. By measuring the long-time $t^{1/2}$ power law, we measure the short-time scaling behavior of the KPZ equation up to a prefactor using Eq. 2.6. Fig. 2.4 shows the tight matching of the asymptotic theory curves and numerically measured values for the variance of $\mathrm{Max}_t^N, \mathrm{Env}_t^N$ and Sam_t^N for a given value of $N = 10^7$. Notice that for $t \approx \log(N)$ the asymptotic theory and numerical values for the variance of Sam_t^N do not fit as well as for large t. This is likely a result of finite-size effects and quickly goes away at

larger values of t or when N increases. The fit for $N = 10^{300}$ in Fig. 2.2 and 2.3 remains tight over the entire range of t.

2.8 Conclusion

The link between RWREs and KPZ universality with its wealth of theoretical, numerical and experimental evidence strongly suggests that aspects of the picture presented here will persist beyond discrete and solvable models, even to experiments. When t is of order $\log(N)$, variances should be non-universal, depending in a difficult to determine way on the nature of the environment. By contrast, when $t \gg \log(N)$, we anticipate that the scaling exponents and functional forms we have identified for the variances of $\mathrm{Env}_t^N, \mathrm{Sam}_t^N$ and Max_t^N will be universal, as will the relation (2.9). The leading coefficients in Eq. (2.7) should be non-universal and hold within them all of the accessible information about the correlation structure of the environment – we call these *extreme diffusion coefficients*. Further theoretical study, such as for the general α, β Beta RWRE model, should provide a natural first test of this universal picture and an understanding of how the extreme diffusion coefficients relate to the microscopic environment. A continuum model that should provide an even wider testing-ground amenable to numerics involves particles $x_i(t)$ for $i = 1, 2, \ldots$ satisfying $dx_i(t) = F(x_i(t), t)dt + D(x_i(t), t)dB_i(t)$ where $F(x,t)$ and $D(x,t)$ are random forcing (as in [53]) and diffusivity (generalizing diffusing diffusivity, c.f. [153]) fields common to all particles while B_i are Brownian motions independent between different i. Changing the correlation structures of F and D will probe the transition between temporally mixing versus quenched environments, which should have very different behavior (c.f. [154, 155]) and warrants further study. Considering higher dimensions as in [53] may lead to further theory that better model real physical systems. A study of higher order

cumulants may reveal other ways to probe the hidden environment, although they may be harder to observe numerically or experimentally.

In physical systems it is impossible to directly measure the environmental variance. However, an indirect measurement can be performed via the approach presented here by using $\delta\text{Env}_t^N \approx \delta\text{Max}_t^N - \delta\text{Sam}_t^N$. The sample variance δSam_t^N is now computed using $\delta\text{Sam}_t^N = \frac{\pi^2 D}{6}\frac{t}{\log(N)}$ where D is the diffusion coefficient. One could repeatedly track the motion of the leading edge of diffusing particles in a system of colloids confined to a quasi-1D channel thereby directly measuring δMax_t^N for system sizes ranging from $N\ 10^2$ to $N\ 10^{10}$. Further, one can also perform complementary measurements on the time of first passage of diffusing objects, which opens the door to experiments done on all manner of diffusing objects, including light or sound diffusing through a scattering medium, dye molecules in a fluid, or any other object whose first passage can be measured. By measuring the environmental variance and extreme diffusion coefficient we will gain a new microscope through which to probe the hidden nature of the underlying environment in which the diffusion occurs. Our work should serve as a guide in the development and analysis of novel experimental measurements of the extreme behavior of many-particle diffusion.

2.9 Acknowledgements

We thank G. Barraquand and P. Le Doussal for discussions and S. Prolhac for providing numerics for $\delta h(0,s)$. This work was funded under the W.M. Keck Foundation Science and Engineering grant on "Extreme Diffusion". I.C. also wishes to acknowledge ongoing support from the NSF through DMS:1811143 and DMS:1937254, the Simon Foundation through a Simons Fellowship in Mathematics (Grant No. 817655), and the Packard Foundation Fellowship for Science and Engineering. Much of this work was performed while I.C. held a Miller Visiting Professorship from the Miller Institute for

Basic Research in Science, and while in residence at the Mathematical Sciences Research Institute in Berkeley, California (NSF Grant No. 1440140). E.I.C. wishes to acknowledge ongoing support from the Simons Foundation for the collaboration Cracking the Glass Problem via award 454939. This work benefited from access to the University of Oregon high performance computing cluster, Talapas.

2.10 Supplementary Material

2.10.1 Numerical Methods.

We expand upon our description of the numerical methods used in our simulations. We consider varying system sizes from $N = 10^2$ to $N = 10^{300}$ with time varying from $t = 0$ to $t = 5000\log(N)$. We simulate such large systems by utilizing the full range of quadruple-precision floating point numbers and making approximations to the binomial distribution when dealing with sizes beyond our precision limits. These approximations are necessary given the limitations of our precision and do not seem to affect the behavior of the system in any significant manner. In particular, for a site x at time t where the number of particles, $N(x,t)$, is below 2^{31} we use the C++ Boost integer implementation of a binomial distributed random number generator to choose the number of particles that will move right versus left. Above 2^{31} the integer implementation overflows and we instead approximate the binomial distribution by a Gaussian distribution of mean $N(x,t)B(x,t)$ and variance $N(x,t)B(x,t)(1-B(x,t))$, as dictated by the central limit theorem. For sufficiently large $N(x,t)$, the variance itself will fall outside of the precision of a quadruple floating point number. This occurs when $N(x,t) > 10^{64}$, above which we approximate the binomial simply by its mean. The number of particles that move right is then $N(x,t)B(x,t)$. Psuodo-code of the simulation is given:

1. Start N particles at $x = 0$

2. For each site:

draw $B(x,t)$ from $\mathscr{U}_{[0,1]}$

if $(N(x,t) > 10^{64})$

$N(x+1,t+1) = N(x,t)B(x,t)$

$N(x-1,t+1) = (1-B(x,t))N(x,t)$

else if $(2^{31} < N(x,t) < 10^{64})$

$\mu = N(x,t)B(x,t)$

$\sigma^2 = N(x,t)B(x,t)(1-B(x,t))$

$N(x+1,t+1)$ is drawn from $\mathscr{N}(\mu,\sigma^2)$

$N(x-1,t+1) = N(x,t) - N(x+1,t+1)$

else if $(N(x,t) < 2^{31})$

$N(x+1,t+1)$ is drawn from $\mathrm{Bin}(N(x,t),B(x,t))$

$N(x-1,t+1) = N(x,t) - N(x+1,t+1)$

where $\mathscr{U}_{[0,1]}$ is the random uniform distribution on the range $[0,1]$, $\mathscr{N}(\mu,\sigma^2)$ is the Gaussian distribution with mean μ and variance σ^2, and $\mathrm{Bin}(n,p)$ is the Binomial distribution with number of trials n and probability p. Note that our simulation differs from Monte Carlo, or agent based, simulations because we can group all the particles at a site together and iterate over each site. Our code is available at https://github.com/CorwinLab/RWRE-Simulations.

When estimating the statistics (e.g. mean and variance) for $\mathrm{Max}_t^N, \mathrm{Env}_t^N$ and Sam_t^N, the optimal manner would be that for each N and t we simulate a large number of environments and then build up histograms for the behavior of these quantities with one data point corresponding to one environment. Of course, in numerically computing the quantities for time t, we naturally compute them for all times smaller than t too, but

for the same environment. Moreover, Env_t^N can be computed simultaneously for all N and t relative to the same environment, providing even further computational savings. We employ this computationally efficient approach to couple together the estimation for different values of N and t to the same pool of environments. There is a cost, however, to doing this. For example, the statistics that we numerically compute for Max_t^N for time t and time t' will themselves be correlated since they are derived from studying the same collection of environments. This correlation seems to be short-lived in time though, and is only evident upon zooming into the numerical measurements, for instances as in the inset in Fig. 2.3 of the main text.

2.10.2 Asymptotic Theory Results.

2.10.2.1 SSRW Max_t^N**.** For the SSRW where $B(x,t) \equiv 1/2$, we use the same notation $p(x,t)$ and $P(x,t)$, dropping the **B** subscript. Now assume that the ratio $\hat{t} = t/\log(N)$ tends to some finite value. As explained in the main article, if $\hat{t} < (\log(2))^{-1}$ then $N \gg 2^t$. In that case, $p(t,t) = 2^{-t} \gg 1/N$ which means that it is highly likely that there are many particles occupying the right-most site at $x = t$. This implies that $\text{Mean}\left(\text{Max}_t^N\right) \approx t$ and $\delta\text{Max}_t^N \approx 0$.

When $\hat{t} > (\log(2))^{-1}$, the maximal random walk at time t will likely occur significantly below t and have non-trivial fluctuations which we now describe. For the SSRW, observe that $p(2k-t,t) = 2^{-t}\binom{t}{k}$ for $k = 0,\ldots,t$. Thus, using Stirling's formula for binomial coefficients (or more generally using Cramer's theorem from the large deviation theory for sums of independent identically distributed random variables) we arrive at the asymptotic for $v \in (0,1)$ that

$$P(vt,t) \approx e^{-tI_{\text{SSRW}}(v)} \quad \text{where} \quad I_{\text{SSRW}}(v) = \frac{1}{2}\big((1+v)\log(1+v) + (1-v)\log(1-v)\big). \tag{2.10}$$

$I_{\text{SSRW}}(v)$ is known of as the large deviation rate function for the SSRW.

We may now combine this with Eq. (2.4) of the main text to show that Max_t^N is approximately distributed as a Gumbel random variable with location $\mu \approx t\hat{v}$ and shape $\beta = 1/I'_{\mathrm{SSRW}}(\hat{v})$, where $\hat{v} = I^{-1}_{\mathrm{SSRW}}(1/\hat{t})$ (here f^{-1} means the inverse function and not the reciprocal). A Gumbel random variable with location μ and shape β has

$$\text{cumulative distribution function } e^{-e^{(-x-\mu)/\beta}}, \quad \text{mean } \mu+\beta\gamma, \quad \text{and variance } \frac{\pi^2}{6}\beta^2, \tag{2.11}$$

where $\gamma \sim .57721$ is the Euler-Mascheroni constant.

To see the above limit, observe that

$$\begin{aligned}&\mathrm{Prob}\big(\mathrm{Max}_t^N \le t\hat{v}+x\big) = \big(1-P_{\mathbf{B}}(t\hat{v}+x,t)\big)^N \approx \big(1-e^{-tI_{\mathrm{SSRW}}(\hat{v}+x/t)}\big)^N\\ &\approx \big(1-e^{-tI_{\mathrm{SSRW}}(\hat{v})-I'_{\mathrm{SSRW}}(\hat{v})x}\big)^N = \big(1-N^{-1}e^{-I'_{\mathrm{SSRW}}(\hat{v})x}\big)^N \approx e^{-e^{-I'_{\mathrm{SSRW}}(\hat{v})x}}.\end{aligned}$$

The first equality follows from Eq. (2.4) of the main text, the second approximation uses (2.10), the third uses Taylor expansion, the fourth follows from the definition of $\hat{v} = I^{-1}_{\mathrm{SSRW}}(1/\hat{t})$, while the final one uses the approximation $(1-x/N)^N \approx e^{-x}$. Notice that in Taylor expanding we have assumed that lower order terms do not cause issues. This can be easily justified by going to further orders in the Stirling formula expansion.

Based on the above Gumbel asymptotics, we can now record the asymptotic form of the mean and variance of Max_t^N for the SSRW. Writing $\hat{v}(\hat{t})$ to make this dependence explicit and recalling that $\hat{t} = t/\log(N)$ we see that

$$\mathrm{Mean}\left(\mathrm{Max}_t^N\right) \approx t\hat{v}\big(\tfrac{t}{\log(N)}\big) + \frac{\gamma}{I'_{\mathrm{SSRW}}\Big(\hat{v}\big(\frac{t}{\log(N)}\big)\Big)}, \quad \delta\mathrm{Max}_t^N \approx \frac{\pi^2}{6\Big(I'_{\mathrm{SSRW}}\Big(\hat{v}\big(\frac{t}{\log(N)}\big)\Big)\Big)^2}. \tag{2.12}$$

Inverting I_{SSRW} to find $\hat{v}(\hat{t})$ is non-trivial though can be done numerically or in certain limits. For instance, noting that for v near zero, $I_{\mathrm{SSRW}} \approx v^2/2$ we see that for $\hat{t}$ near infinity, $\hat{v}(\hat{t}) \approx \sqrt{2/\hat{t}}$ and hence $I'_{\mathrm{SSRW}}\big(\hat{v}(\hat{t})\big) \approx \sqrt{2/\hat{t}}$. From this and (2.12) it follows

that for $\hat{t} \gg (\log(2))^{-1}$, asymptotically

$$\text{Mean}\left(\text{Max}_t^N\right) \approx \left(\sqrt{2\log(N)} + \frac{\gamma}{\sqrt{2\log(N)}}\right)t^{1/2}, \qquad \delta\text{Max}_t^N \approx \frac{\pi^2}{12}\frac{t}{\log(N)}.$$

On the other hand, (2.12) also shows that as $\hat{t}$ tends to $(\log(2))^{-1}$ from above, the mean goes to t and the variance goes to zero.

2.10.2.2 RWRE Env_t^N**.** Assume that the ratio $\hat{t} = t/\log(N)$ tends to some finite value exceeding 1. The key theoretic result we use here is due to [52]. They show that for $v \in (0,1)$,

$$\log\left(P_{\mathbf{B}}(vt,t)\right) = -tI(v) + t^{1/3}\sigma(v)\chi_t \quad \text{where} \quad I(v) = 1-\sqrt{1-v^2}, \quad \sigma(v) = \left(\frac{2I(v)^2}{1-I(v)}\right)^{1/3}. \tag{2.13}$$

Here $I(v)$ is the large deviation rate function and $\sigma(v)t^{1/3}$ is the scalings of the random environment-dependent fluctuations χ_t around that rate function. [52] showed that as $t \to \infty$, the distribution of χ_t converges to a Tracy-Widom GUE distribution χ. For reference below, let us note that [152]

$$\mu_\chi := \text{Mean}\,(\chi) \approx -1.771, \qquad \sigma_\chi^2 := \delta\chi \approx .813.$$

As in the case of the SSRW, we now solve for $\hat{v} = \hat{v}(\hat{t})$ such that $P_{\mathbf{B}}(\hat{v}t,t) = 1/N$. Note that $\hat{v}t$ will then equal the $1/N$-quantile Env_t^N. From (2.13), $\hat{v}$ must satisfy

$$tI(\hat{v}) - t^{1/3}\sigma(\hat{v})\chi_t = \log(N) = t/\hat{t}. \tag{2.14}$$

Canceling t and dropping the $t^{1/3}$ term momentarily yields to first order that $\hat{v}$ is given by

$$\hat{v}_0 = I^{-1}(1/\hat{t}) = \sqrt{1-(1-1/\hat{t})^2}.$$

We can now Taylor expand $I(\hat{v})$ and $\sigma(\hat{v})$ in (2.14) around $\hat{v} = \hat{v}_0$ and solve for $\hat{v}$ to the next order. Doing so we find that

$$\hat{v} = \hat{v}_0 + t^{-2/3}\frac{\sigma(\hat{v}_0)}{I'(\hat{v}_0)}\chi_t + O(t^{-4/3}).$$

Recalling that $\hat{v}t$ is supposed to yield the $1/N$-quantile, we conclude that

$$\mathrm{Env}_t^N = \hat{v}_0 t + t^{1/3}\frac{\sigma(\hat{v}_0)}{I'(\hat{v}_0)}\chi_t + O(t^{-1/3}). \tag{2.15}$$

From this we can extract the asymptotic mean and variance of Env_t^N. Written explicitly (i.e., plugging in I and $\hat{v}_0$) this yields the following asymptotic formulas

$$\mathrm{Mean}\left(\mathrm{Env}_t^N\right) \approx M_1(N,t) := \left(1-\left(1-\tfrac{\log(N)}{t}\right)^2\right)^{1/2} t + (\log(N))^{2/3}t^{-1/3}\frac{2^{1/3}\left(1-\frac{\log(N)}{t}\right)^{2/3}}{\sqrt{1-\left(1-\frac{\log(N)}{t}\right)^2}}\mu_\chi$$

$$\delta\mathrm{Env}_t^N \approx V_1(N,t) := \left(\frac{(\log(N))^{4/3}}{t^{2/3}}\right)\frac{2^{2/3}\left(1-\frac{\log(N)}{t}\right)^{4/3}}{1-\left(1-\frac{\log(N)}{t}\right)^2}\sigma_\chi^2,$$

where above we have used that

$$\frac{\sigma(\hat{v}_0)}{I'(\hat{v}_0)} = \frac{2^{1/3}\hat{t}^{-2/3}(1-1/\hat{t})^{2/3}}{\sqrt{1-(1-1/\hat{t})^2}}.$$

For $\hat{t} = t/\log(N)$ large, it follows from the above expressions that

$$\delta\mathrm{Env}_t^N \approx \sigma_\chi^2\left(\tfrac{\log(N)}{2}\right)^{\frac{1}{3}} t^{\frac{1}{3}}. \tag{2.16}$$

It is important to understand the order of the limits here. First we should fix $\hat{t} = t/\log(N)$ and take N and t to infinity. Then we take $\hat{t}$ large and find the above $1/3$ power-law. That said, with some additional work using the methods of [52] it is possible to show that for the entire range $1 \ll t/\log(N) \ll \log(N)$, this $1/3$ power-law persists. We will not provide the details for that here. However, below we will consider when t is of order $(\log(N))^2$. In that case, for small t in that range, we will find a perfect fit to the $1/3$ power-law, thus agreeing with the assertion that this power-law persists over the full range $1 \ll t/\log(N) \ll \log(N)$.

Now assume that the ratio $\hat{\hat{t}} = t/\log(N)^2$ remains strictly positive and finite as N and t tend to infinity. While [52] probes $P_{\mathbf{B}}(x,t)$ for x linearly growing with t, [132] probes the regime where x grows like $t^{3/4}$. They show that for $v \in (0,\infty)$,

$$\log\left(P_{\mathbf{B}}(vt^{3/4},t)\right) \approx -\frac{v^2t^{1/2}}{2} - \frac{\log(t)}{4} + \log(v) - \frac{v^4}{12} + h(0,v^4) \tag{2.17}$$

where $h(y,s)$ denotes the (random) height at spatial position y and time s of the *narrow wedge solution to the Kardar-Parisi-Zhang (KPZ) equation*

$$\partial_s h(y,s) = \tfrac{1}{2}\partial_y^2 h(y,s) + \tfrac{1}{2}\big(\partial_y h(y,s)\big)^2 + \xi(y,s)$$

driven by space-time white noise ξ, see [129, 133]. Using this result, we will be able to prove this other $(\log(N))^2$ time scale.

We may solve (2.17) perturbatively (as in the $\log(N)$ case) for $\hat{\hat{v}}$ such that $P_{\mathbf{B}}(\hat{\hat{v}}t^{3/4},t) = 1/N$. The $1/N$-quantile $\mathrm{Env}_t^N = \hat{\hat{v}}t^{3/4}$ is then given by

$$\mathrm{Env}_t^N \approx \hat{\hat{v}}_0 t^{3/4} + \frac{t^{1/4}}{\hat{\hat{v}}_0}\left(h(0,\hat{\hat{v}}^4) - \frac{\hat{\hat{v}}_0^4}{12} - \log\big(\hat{\hat{v}}_0\big)\right) + O(t^{-1/4}) \quad \text{where} \quad \hat{\hat{v}}_0 = 2^{1/2}\hat{\hat{t}}^{-1/4}.$$

From this we can explicitly compute the asymptotics of the mean and variance as

$$\begin{aligned}\mathrm{Mean}\left(\mathrm{Env}_t^N\right) &\approx M_2(N,t) := \big(2t\log(N)\big)^{1/2} + \sqrt{\tfrac{t}{2\log(N)}}\,\mathrm{Mean}\left(h\Big(0,\tfrac{4(\log(N))^2}{t}\Big)\right)\\ \delta\mathrm{Env}_t^N &\approx V_2(N,t) := \tfrac{t}{2\log(N)}\cdot\delta h\Big(0,\tfrac{4(\log(N))^2}{t}\Big).\end{aligned} \tag{2.18}$$

Notice that in the mean we have dropped the lower order contributions from the terms $\frac{\hat{\hat{v}}_0^4}{12}$ and $\log\big(\hat{\hat{v}}_0\big)$. The values of $\mathrm{Mean}\,(h(0,s))$ and $\delta h(0,s)$ for varying $s>0$ can be computed numerically through evaluation of the Fredholm determinant formula from [134–137]. The result of this computation is recorded as Fig. 3 of [147]. In particular, the horizontal axis (labeled t in [147]) corresponds to our s variable, and the red circles record the value of $\mathrm{Mean}\left(\frac{h(0,s)+\frac{s}{24}}{(s/2)^{1/3}}\right)$ while the blue triangles record the values of $\delta\frac{h(0,s)+\frac{s}{24}}{(s/2)^{1/3}}$ (note that the $s/24$ shift here does not change the variance as it is deterministic). For $s>.33$ we approximate the mean and variances by interpolating between the numerically evaluated values in [147] (S. Prolhac kindly provided the data set used to create Fig. 3 in that paper). For $s<.33$ we use the short-time behavior of the KPZ equation explained below for our values of the mean and variance.

There are two key asymptotics for $h(0,s)$ derived in [134–137]: $\frac{h(0,s)+\frac{s}{24}}{(s/2)^{1/3}} \approx \chi$ as $s\to\infty$ where χ is a Tracy-Widom GUE distributed, and $h(0,s) \approx -\frac{1}{2}\log(2\pi s) +$

$s^{1/4}\pi^{1/4}2^{-1/2}G$ as $s \to 0$ where G is standard Gaussian distributed. These imply corresponding asymptotics for the mean and variance. In particular, as $\hat{\hat{t}} \to 0$,

$$\delta\mathrm{Env}_t^N \approx \sigma_\chi^2 2^{-1/3}\log(N)\hat{\hat{t}}^{1/3} = \sigma_\chi^2\left(\tfrac{\log(N)}{2}\right)^{\frac{1}{3}} t^{\frac{1}{3}}$$

which agrees perfectly with (2.16). This shows that the long-time behavior in the $t = O(\log(N))$ scaling regime and the short time behavior in the $t = O(\log(N)^2)$ scaling regime match even up to the pre-factor. This strongly suggests the $1/3$ power-law in Eq. **??** of the main text for the entire regime $1 \ll t/\log(N) \ll \log(N)$.

On the other hand, from the short-time KPZ asymptotic we find that as $\hat{\hat{t}} \to \infty$,

$$\delta\mathrm{Env}_t^N \approx \frac{1}{2}\pi^{1/2}t^{1/2}$$

thereby recovering Eq. (2.7) for the regime $t \gg (\log(N))^2$ in the main text. This indicates that for finite N and t it is necessary to stitch together the two regimes to get a reasonable formula for $\delta\mathrm{Env}_t^N$. We have found that an error function centered at $t = (\log(N))^{3/2}$ with a width of $(\log(N))^{4/3}$ produces a smooth transition between the two regimes. Thus, our final expression for the asymptotic mean and variance is given by

$$\mathrm{Var}^{\mathrm{asy}}\left(\mathrm{Env}_t^N\right) = \frac{1-\mathrm{erf}\left(\frac{t-(\log(N))^{3/2}}{(\log(N))^{4/3}}\right)}{2}V_1(N,t) + \frac{1+\mathrm{erf}\left(\frac{t-(\log(N))^{3/2}}{(\log(N))^{4/3}}\right)}{2}V_2(N,t), \quad (2.19)$$

provided that $t \geq \log(N)$ and 0 for $t < \log(N)$. Here $\mathrm{erf}(x) = 2/\sqrt{\pi}\int_0^x e^{-t^2}dt$ is the error function. This construction is shown in Fig. 2.6. On the other hand, such stitching is unnecessary when it comes to the mean since the large t behavior of $M_1(N,t)$ matches the behavior of $M_2(N,t)$ all the way as $t \to \infty$. This can be seen through direct asymptotics of the formulas and is illustrated in Fig. 2.5. On this account, we simply take

$$\mathrm{Mean}^{\mathrm{asy}}\left(\mathrm{Env}_t^N\right) = M_1(N,t). \quad (2.20)$$

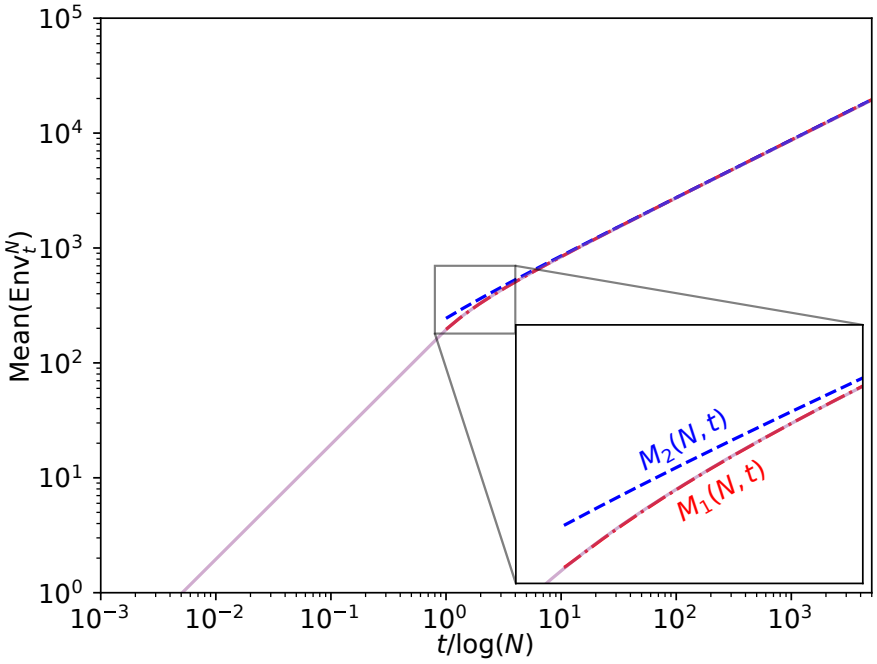


Figure 2.5. The asymptotic mean functions $M_1(N,t)$ and $M_2(N,t)$ are plotted for $N = 10^{85}$ in red and blue dashed lines, respectively. They agree closely for the full range of $t > \log(N)$ and also match the numerically measured values $\text{Mean}^{\text{num}}\big(\text{Max}_t^N\big)$ given by the purple curve (which is linear, as expected, until roughly time $t = \log(N)$).

2.10.2.3 ***RWRE*** Sam_t^N ***and*** Max_t^N**.** Assume for the moment that $t = \hat{t}\log(N)$ for $\hat{t} > 1$. Then (2.13) implies that

$$P_{\mathbf{B}}(\text{Env}_t^N + x, t) = \exp\Big(-tI\big(\tfrac{\text{Env}_t^N}{t} + \tfrac{x}{t}\big) + t^{1/3}\sigma\big(\tfrac{\text{Env}_t^N}{t} + \tfrac{x}{t}\big)\chi_t \Big) \qquad \text{and} \quad P_{\mathbf{B}}(\text{Env}_t^N, t) = \frac{1}{N}.$$

If we Taylor expand to the next order in the exponential we find

$$\begin{aligned} P_{\mathbf{B}}(\text{Env}_t^N + x, t) &\approx \exp\Big(-tI\big(\tfrac{\text{Env}_t^N}{t}\big) - I'\big(\tfrac{\text{Env}_t^N}{t}\big)x + t^{1/3}\sigma\big(\tfrac{\text{Env}_t^N}{t}\big)\chi_t \Big) \\ &= \frac{1}{N} e^{-I'\left(\frac{\text{Env}_t^N}{t}\right)x} \approx \frac{1}{N} e^{-I'(\hat{v}(\hat{t}))x}. \end{aligned}$$

The Taylor expansion requires a bit of explanation. We expand $I\big(\frac{\text{Env}_t^N}{t} + \frac{x}{t}\big) \approx I\big(\frac{\text{Env}_t^N}{t}\big) + I'\big(\frac{\text{Env}_t^N}{t}\big)\frac{x}{t}$ to first order. The similar expansion of σ would produce a lower order term. However, there is a subtlety that we should point out. The χ_t random variable implicitly depends on x as well. Namely, if we look at the random transition probability as we vary

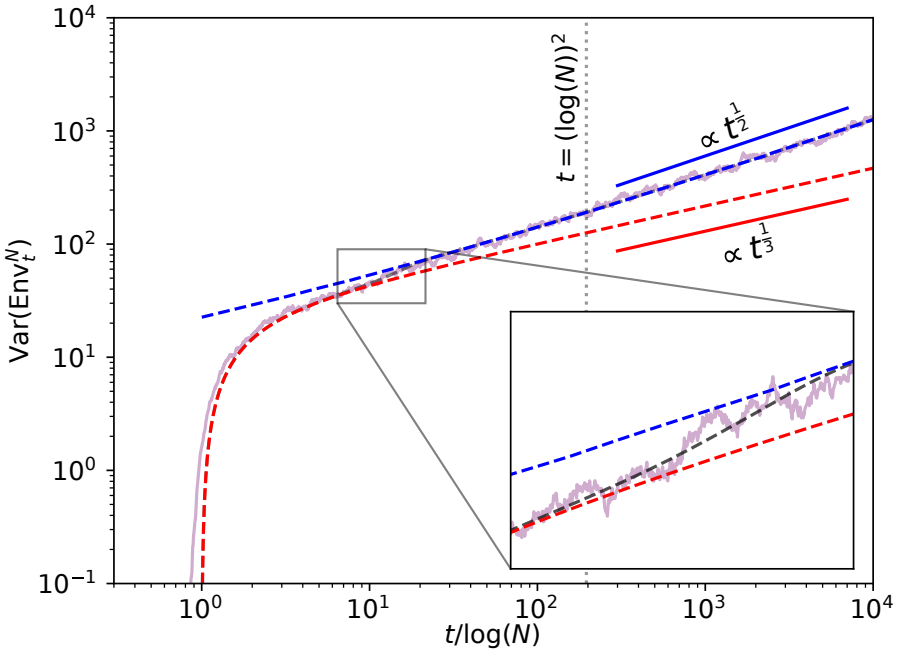


Figure 2.6. The asymptotic variance functions $V_1(N,t)$ and $V_2(N,t)$ are plotted for $N = 10^{85}$ in red and blue dashed lines, and the stitched together formula for $\mathrm{Var}^{\mathrm{asy}}\left(\mathrm{Env}_t^N\right)$ from (2.19) is plotted as the black dashed line. The purple curve is the numerically measured curve $\mathrm{Var}^{\mathrm{num}}\left(\mathrm{Env}_t^N\right)$. The inset shows how the stitching captures the transition between the two asymptotic curves V_1 and V_2, and the solid lines show the asymptotic power-laws that V_1 and V_2 demonstrate as $t \to \infty$. The vertical dotted line indicates the regime crossover at $t = (\log(N))^2$.

around Env_t^N, the fluctuations of this quantity will vary with x. However, we assume here that this fluctuation does not contribute to leading order. This assumption would be true if, for instance, χ_t looked locally like a random walk with independent and identically distributed intervals. This property is believed to be universal to models in the KPZ class and thus it is reasonable to assume that the same holds here. We do not attempt to justify this theoretically beyond this heuristic, though note that it yields very good agreement with our numerical simulations. The final approximation in the above string of equations involves replacing $I'\left(\frac{\mathrm{Env}_t^N}{t}\right)x$ by $I'(\hat{v}(\hat{t}))x$ which relies on the fact that $\frac{\mathrm{Env}_t^N}{t} \approx \hat{v}_0$ to highest order.

Combining the above deduction with (**??**) in the main text and $(1-x)^N \approx e^{-xN}$ (for x small) yields

$$\text{Prob}(\text{Max}_t^N \leq \text{Env}_t^N + x) \approx \left(1 - \frac{1}{N} e^{-I'(\hat{v}(\hat{t}))x}\right)^N \approx e^{-e^{-I'(\hat{v}(\hat{t}))x}}. \tag{2.21}$$

If we define Sam_t^N by the equality $\text{Max}_t^N = \text{Env}_t^N + \text{Sam}_t^N$ then the above calculation shows that Sam_t^N is asymptotically independent of Env_t^N and asymptotically is Gumbel distributed with location and shape parameters

$$\mu(t) = 0, \qquad \beta(t) = 1/I'(\hat{v}(\hat{t})) = (\hat{t}-1)(2\hat{t}-1)^{-1/2} \approx (\hat{t}/2)^{1/2}$$

where the approximation is for $\hat{t} \gg 1$. This justifies the addition law for variances (Eq. (**??**) in the main text)

$$\delta\text{Max}_t^N \approx \delta\text{Env}_t^N + \delta\text{Sam}_t^N \tag{2.22}$$

and (using the Gumbel variance formula in (2.11)) this also justifies Eq. (**??**) of the main text which provides the asymptotic formula for the variance (we also record that the asymptotic mean is 0)

$$\text{Mean}^{\text{asy}}\left(\text{Sam}_t^N\right) = 0, \qquad \text{Var}^{\text{asy}}\left(\text{Sam}_t^N\right) = \frac{\pi^2}{6} \frac{\left(\frac{t}{\log(N)} - 1\right)^2}{2\frac{t}{\log(N)} - 1} \approx \frac{\pi^2}{12} \frac{t}{\log(N)}, \tag{2.23}$$

where the approximation is for $\hat{t} \gg 1$.

Putting together (2.19), (2.20), (2.22) and (2.23) we conclude that

$$\begin{aligned} \text{Mean}^{\text{asy}}\left(\text{Max}_t^N\right) &= M_1(N,t), \\ \text{Var}^{\text{asy}}\left(\text{Max}_t^N\right) &= \frac{1 - \text{erf}\left(\frac{t-(\log(N))^{3/2}}{(\log(N))^{4/3}}\right)}{2} V_1(N,t) + \frac{1 + \text{erf}\left(\frac{t-(\log(N))^{3/2}}{(\log(N))^{4/3}}\right)}{2} V_2(N,t) \\ &\quad + \frac{\pi^2}{6} \frac{\left(\frac{t}{\log(N)} - 1\right)^2}{2\frac{t}{\log(N)} - 1}. \end{aligned} \tag{2.24}$$

The above calculation assumed $\hat{t} = t/\log(N)$ converges to a finite value. However, in a similar manner based on (2.17) we can probe the behavior when $\hat{\hat{t}} = t/(\log(N))^2$ converges to a finite value. This behavior agrees perfectly with the large $\hat{t}$ limiting

behavior above. Thus, we conclude that the formula for $\mathrm{Var}^{\mathrm{asy}}\left(\mathrm{Sam}_t^N\right)$ should hold for all $t \gg \log(N)$.

Fig. 2.7 show our asymptotic theory formulas for the mean of the maximal particle fit closely with our numerical simulations.

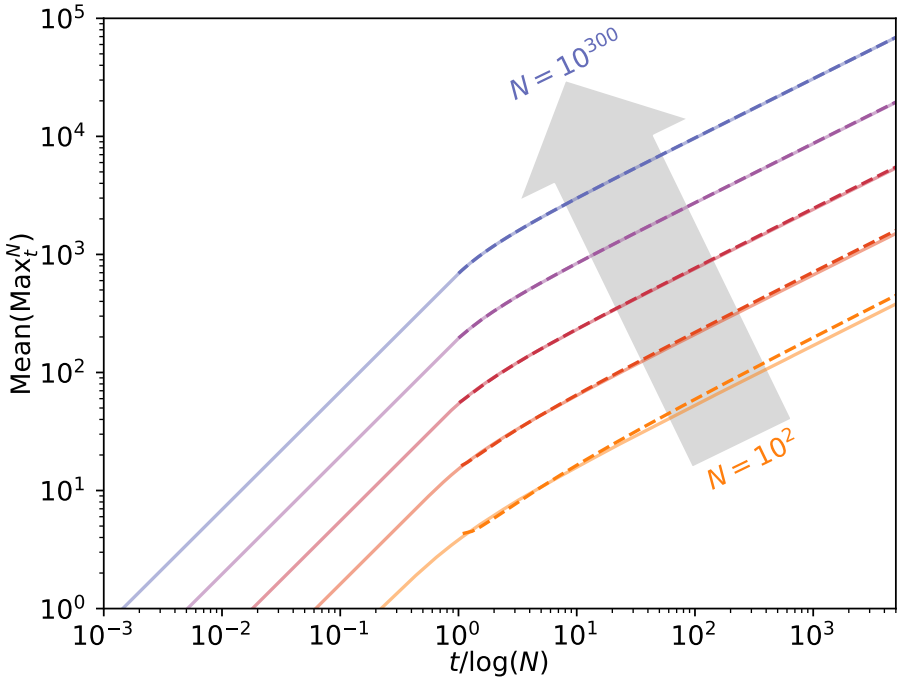


Figure 2.7. The mean position of the maximal particle location (solid line) for $N = 10^2, 10^7, 10^{24}, 10^{85}$ and 10^{300} for 10000, 5000, 1000, 500 and 500 instantiations of the environment, respectively. The theoretical prediction (dashed line) given in Eq. (2.24) is also shown. We find the theoretical predictions for the mean position of the maximum particle, $\mathrm{Mean}\left(\mathrm{Max}_t^N\right)$, are in agreement with the data.

CHAPTER III

MEASUREMENTS OF EXTREME FIRST PASSAGE TIMES IN COLLOID SUSPENSIONS

3.1 Introduction

Understanding the outliers in diffusive processes is the key to describing many important phenomena, such as biological processes dependent on the interactions between strands of DNA [156], a wide variety of biological and chemical processes [36, 56, 58–60], and how microscopic price fluctuations relate to long-term macroscopic trends in the stock market [54, 55]. How do we predict the behavior of these furthest or fastest particles? In diffusive environments, where many particles spread outward from their originating source, we typically use Einstein's treatment of diffusion to describe the bulk behavior of the particles [26–28]. Einstein described diffusion as particles undergoing independent random walks, but the independent nature of these walks ignores the effect the shared environment has on the particles. As a result, when analyzing the system as a whole, the distributions of outlier particle locations and extreme first passage times should differ from those predicted by Einstein's theory. Instead, we can use a biased random walk to describe the system, as in the numerical work done in Chapter II. To build on these numerical predictions, here we propose an experimental setup to measure distributions of extreme first passage times in a real, physical system.

3.2 Background

While the classical Einstein independent random walk model describes the average behavior well in many systems, there are areas where this theory and its predictions are known to fail. For example, Brownian motion in supercooled liquids and close to jamming [46], systems with active matter that adds energy into the environment [43, 44], or those described by Lévy flights and other anomalous diffusion

processes better describe the dynamics [45, 47**?** , 48] have probability distributions that display exponential tails and other non-Gaussian characteristics and exhibit significant differences for the extreme particles. Chapter II builds on a theoretical model for diffusion that explicitly includes correlations resulting from the shared background environment by modelling diffusion as a random walk with transition probabilities drawn from the beta distribution [52]. The Barraquand-Corwin model predicts the behavior of the maximum of a large number of "walkers", the particle farthest from the origin at a given time, and reveals a connection to the Kardar-Parisi-Zhang universality class with a related phase transition [52, 53, 83, 132, 133].

Measurements of the time of *first* first passage, the extreme first passage time (EFPT), in physical systems have the potential to unlock new insights into the shared underlying medium of the diffusing particles. An experimental system to image and track colloidal particles diffusing through quasi-1D glass capillary tubes would enable us to measure EFPTs in a real diffusive system. By filling a capillary tube with a colloidal microsphere suspension, centrifuging all colloids to one end of the tube, and then imaging the tubes under a microscope throughout time, we can determine the time it takes the first of all colloids to diffuse to a certain point within the microscope field of view. In order to measure the EFPT variance, we have to do this for many colloidal suspensions. By centrifuging and subsequently collecting concurrent time lapse imaging for multiple capillaries, we can collect many EFPTs in each experimental run. We can then repeat this process until we gather a statistically significant number of EFPTs, and measure the mean and variance of the EFPT distribution. We can alter the properties of the system and explore how adjusting experimental parameters alters these EFPT distributions and their statistics.

Recent theoretical and numerical developments in characterizing EFPTs of systems diffusing in random environments describe an asymptotic theory for how the variance in EFPT scales with particle number N and path length L, from systems exceeding $N = 10^{28}$ particles down to $N = 100$ particles [84]. As in Chapter II, which considered extreme particle location, this numerical work found that measurements of the EFPT allows us to separate out information about the random environment from the sampling trajectories within it. For large N systems of path length L, the variance is proportional to $\frac{L^4}{(\ln(N))^4}$, and by calculating and subtracting off the sampling variance, one can determine the environmental variance, which should scale as $\frac{L^3}{(\ln(N))^{\frac{5}{2}}}$ [84]. By varying the concentration of colloids in the capillaries, we can control the number of diffusing colloids, and measure the relationship between the system size and EFPT statistics.

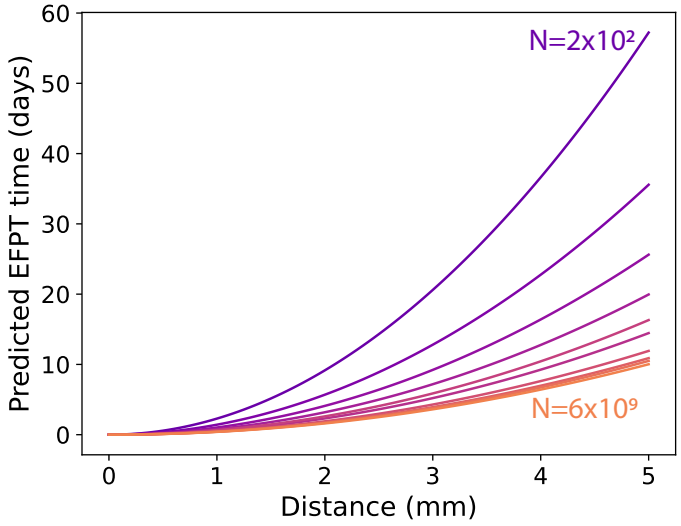


Figure 3.1. Predicted extreme first passage times for $d = 1.18\ \mu$m silica colloids suspended in water at room temperature diffusing across distances up to 5mm from the origin. EFPT predictions from the origin to a distance L of 5mm vary from around 10 days for a system of $N = 5 \times 10^9$ colloids (25% colloids by weight) to nearly 60 days for $N = 2 \times 10^2$ colloids.

We can predict the EFPTs we expect to see in a system of some number of colloidal microspheres N by calculating the diffusion coefficient D and using the

probability of the position $B(t)$ of a Brownian walker to be found beyond distance L at time t, given by

$$P(B(t) > L) = 1 - \text{erf}\left(\frac{L}{2\sqrt{Dt}}\right) \tag{3.1}$$

to solve for the value of t where this probability exceeds $1/N$ [56]. Figure 3.1 displays predicted EFPT to distances ranging from 0-5mm for systems of $d = 1.18$ μm silica colloids suspended in water, with system sizes ranging from $N \approx 10^2 - 10^9$. We can use data collected with various concentrations of colloids to determine, for a given value of L, how the system size N affects the EFPT variance and whether the anticipated $\frac{L^3}{(\ln(N))^{\frac{5}{2}}}$ scaling emerges. We can also use the same data repeatedly to ensure the results hold across L values varying based on the microscope field of view.

Additionally, recent work (in review) on diffusion in random environments also reveals a connection between the variance of the EFPT and an *extreme* diffusion coefficient, providing an additional characterization of the fluctuations of the shared hidden environment made through measurements of the extreme particle statistics [157]. While the regular Einstein diffusion coefficient is determined by particles' average step size, this extreme diffusion coefficient is determined through the variance in both size and direction of a single step resulting from fluctuations in the environment. By changing the properties of the colloids and the medium in which they are suspended, which affect both the Einstein diffusion coefficient and EFPT statistics, we explore any additional changes in the extreme diffusion coefficient and determine its efficacy in better describing these systems. Varying colloid size and material, using fluids of different viscosities, and altering the electrical properties of the particles in suspension all result in changes to the diffusion coefficient. By measuring the effect of these both on the EFPT and the extreme diffusion coefficient, countless new insights into the underlying physical process of diffusion and how we describe and make predictions for these systems could be accessed.



Figure 3.2. Render of the experimental setup, using CAD designs. The centrifuge base plate, rotor plate, support arm, and braces were designed and machined specifically for use with the motor, rotary encoder, and tachometer. The rotor plate is designed with 16 channels of two depths, fabricated on a CNC mill for precision, allowing different capillary widths to rest securely in the plate. Circular holes allow light from the microscope to pass through the capillaries for imaging. While the capillaries may be up to 100mm long, only the first few millimeters from the outer edge can be imaged; see Figure 3.1, where such distances correspond to EFPTs on the order of multiple days or even weeks. The microscope shown is an approximate model of the Nikon Eclipse FN-1 used in this experiment, with a camera attached to the C-mount.

3.3 Experimental design

To accurately measure EFPTs in suspensions of colloidal microspheres, we require as high precision as is feasibly possible on capillary positioning – in practice, this is down to a few millimeters. In fabricating the rotor plate, we used high precision CNC milling machines and procedures, easy-to-machine cast aluminum to ensure the plate was as flat as possible, designed the system symmetrically, and took great care to ensure the rotor plate was extremely level once assembled to avoid gravity-driven flow inside the capillaries. It is important that the colloids be density matched well enough that they do not sediment quickly due to gravity, but can still be centrifuged in a reasonable time limit. Silica was chosen because its density is approximately 2 times that of water, which delays its sedimentation under gravity while completely centrifuging to the capillary edge in well under 30 minutes at the rotor's top speed. Additional work can be done in image analysis and post processing to localize particles with high precision. To avoid missing any colloids in the imaging process, we balance the magnification strength with the resulting depth of field to maximize the number of colloids in focus, use colloids with a mismatched index of refraction from the medium, use the lowest possible numerical aperture, and select very thin and narrow (varying from 0.2-0.4mm x 2-4mm dimensions) flat rectangular capillaries. Initial data has been collected at 10x magnification, which allows the majority of the 1μm particles in the solution to be visualized under the microscope. If this does not provide enough depth of field, 4x magnification and subpixel resolution particle localization methods could potentially be used to retrieve enough information for EFPT measurement [158].

The microscope-centirfuge system developed under these considerations is shown in Figure 3.2. The centrifuge consists of a flat rotor plate, which holds 16 samples inside small windows left open for imaging, fixed to a DC motor (McMaster-Carr 59835K62)

via screw-clamp bushing (McMaster-Carr 5926K16). The angular position of the plate is encoded through the use of an incremental optical rotary motion encoder (McMaster-Carr, 9749T2). A tachometer is used to record angular velocity, creating a type 2 servo system and thereby achieving translational positioning precision down to 3mm. A 12V sealed linear solenoid (McMaster-Carr 69905K173) acts as a brake to assist in final position stabilization. An aluminum base plate and support provide stability by bolting the entire system into an optics table. A microcontroller (Arduino Mega) runs an analog servo system, using a total of 19 digital pins, where 3 pins each trigger the brake, run the centrifuge at full speed, and turn the servo mode on or off. In servo mode, the remaining 16 digital pins write the centrifuge to a 16-bit location. The centrifuge speed can exceed 1000 RPM and effectively sediments samples of silica microspheres inside the capillary tubes as required.

An upright fixed stage microscope (Nikon ECLIPSE FN1) with a 10x objective, with a camera (Teledyne Blackfly S USB3) connected to the C-mount, is used to image silica microsphere (Cospheric monodisperse silica microspheres, 1.18 μm diameter, 2.5% coefficient of variation) suspensions in deionized water. Suspensions are typically around 1% silica by weight, and are sonicated upon formulation to disperse aggregates. In future work, the concentration should be varied to control the number of diffusing colloids N. We coat the interior of 100mm long rectangular capillary tubes (Vitrocom VitroTubes™ 5003, 5004), 0.3mm/0.4mm wide and 0.03mm/0.04mm tall, with bovine serum albumin (BSA), flushing out the excess with pressurized air. This interior coating helps prevent microspheres from adhering to the capillary walls. We then fill the tubes with the silica suspensions, break off any tube portions containing visible air pockets, and seal the ends with capillary wax (Sigillum wax sealant). We dip the ends in cyanoacrylate glue to provide a strong seal for when the centrifuge spins the samples at high speeds. The

capillary surface is then gently cleaned with isopropyl alcohol and lens paper and placed into its channel in the rotor plate. This process is repeated for 16 capillary tubes, taking care to ensure the capillaries are placed as level as possible to prevent gravity-driven flow. Melted paraffin wax is carefully poured onto the non-imaging parts of each capillary, which, once cooled, adheres the capillaries in place in the channel.

A MATLAB script, located at the end of this chapter in Section 3.6, controls both the Arduino for centrifuge operation and the camera for imaging. Upon starting the script, the Arduino pins and USB camera are initialized, and directories based on the date and time of initialization are created for data storage. The centrifuge enters “run” mode for a preset amount of time, where it spins at the highest attainable speed. After the time runs out, the centrifuge slows down, switches to “servo” mode, and the 16 position pins send it to the "16th" capillary location for consistent positioning. The centrifuge then carefully pans through each of the capillary locations, collecting an initial "reference" image of each one. After the user verifies that all capillaries are in frame and that the centrifuge process has been successful, the script enters time-lapse mode. On a preset time interval, the centrifuge pans through each location and collects a new frame for each capillary. Each frame is stabilized relative to its initial "reference" frame and the stabilized image is written to an image file inside that capillary’s image directory. After cycling through each capillary, the system pauses for the allotted time interval, then cycles through to collect and stabilize frames again. This process repeats until the user ends this sequence, and the final parts of the script close the camera and clear all variables for the next collection.

3.4 Preliminary results

To date, this work has demonstrated that it is possible to centrifuge down samples in capillary tubes such that the majority of the colloids end up on the outer end and utilize microscopy to record colloid movement a given distance from that outer edge.

By removing air bubbles beforehand, and coating the tubes with bovine serum albumin, we minimize bulk flow and colloids sticking to the glass. Image stabilization removes discrepancies in the servo positioning and enables tracking of particles using packages such as Trackpy. Work remains to be done in determining the appropriate time lapse intervals to keep particles linked between frames while minimizing the amount of data that must be stored for each experimental run.

Figure 3.3 displays two example frames from the same capillary at different points of the time lapse. After 15 hours, a large number of colloids have entered the frame from the upper left corner. This is significantly quick for bulk flow undergoing only diffusion, and indicates that there are likely other factors involved creating net movement inside the capillary.

Preliminary work on image processing can be seen in Figure 3.4, using the chronologically later frame (right) in 3.3. By increasing contrast and using filtering, we can make individual colloids stand out more against the background and improve the conditions for using localization and tracking methods. More work can be done to select the optimal methods for reducing noise, eliminating the background, removing

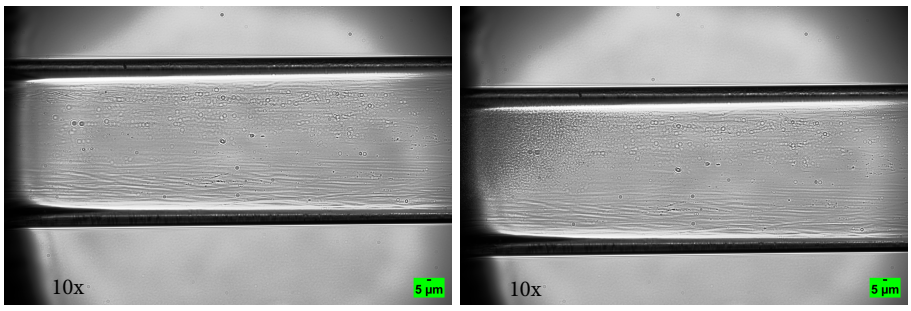


Figure 3.3. Examples of imaged capillary at start of time lapse and 300 frames later. Colloids enter from the top left corner, suggesting that the capillary was placed at a slight angle and that gravity is drawing colloids to the upper capillary wall.

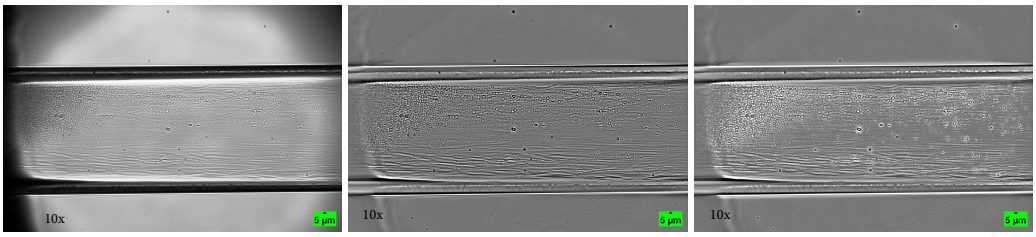


Figure 3.4. Examples of edits that can be made to highlight features in images of capillaries. The left image has had the contrast increased, the center image has also been run through a bandpass filter, and the right image has additionally had the brightest pixels enhanced via the ImageJ Maximum filter.

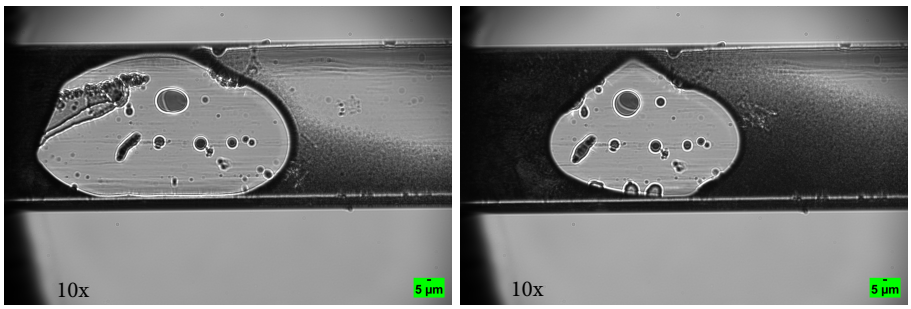


Figure 3.5. Examples of an air bubble inside a capillary, and how it affects colloid centrifuging and diffusion. The left frame was captured immediately after centrifuging, and the right frame was taken approximately 50 hours later.

spurious colloids stuck to the glass, highlighting moving colloids, and dealing with other imperfections that arise throughout the time lapse.

In Figure 3.5 and 3.6, we see a few of the major barriers to collecting accurate diffusive EFPTs. The air pocket in Figure 3.5 prevented the colloids from sedimenting at the outer end of the capillary, and introduces additional forces on the fluid and colloids that prevent simple diffusion from being the only process creating translational movement. This issue is mitigated by removing air pockets visible when filling the capillary. Figure 3.6 shows the more prevalent and difficult to resolve issues impeding progress; from capillaries placed unknowingly at an angle, to error in servo positioning leaving part or all of the capillary out of the field of view, to capillaries not flush with the

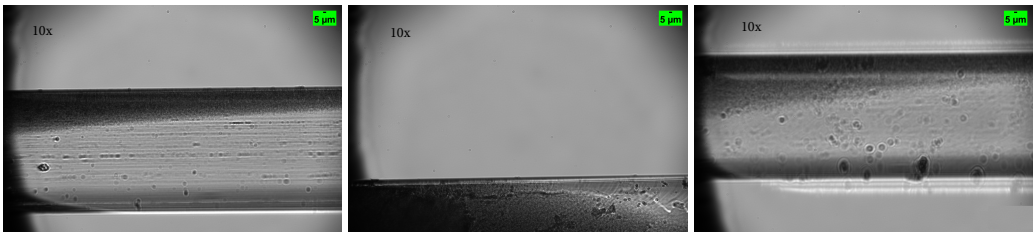


Figure 3.6. Other issues encountered include capillaries placed at an angle (left), servo positioning failures (center), and capillaries that are disturbed from the original placement and end up out of the microscope focus (right).

very bottom of the rotor channels, it can still be difficult to eliminate gravity-driven flows and ensure that imaging can be done as accurately as possible. By running a check before sealing capillaries in place with wax, some of these errors can be mitigated; however, it can be unclear that capillaries are angled and the centrifuge process can still introduce enough unwanted movement to displace one or two of them from the focal point.

Finally, it is unclear exactly what distance the microscope field of view is from the origin, or what the "origin" is in a system of colloids sedimented at the far end of a capillary. It is clear from Figure 3.1 that even very minute differences should play a significant role in resulting EFPTs. With large system sizes, we cannot assume all particles are starting from the exact same location. How much uncertainty does this introduce into the final EFPT? How can we factor this error in starting position into the total calculation of L? Is the distance from origin to L large enough that it doesn't matter? Is the distance from origin to L too small to use the results from the EFPT numerical work [84, 157]? Is the distance from origin to L too large to even get results without bulk flow driving particles outside of simple diffusion? Can drift be accounted for within the theoretical framework? These questions, and undoubtedly countless others, are currently unanswered and introduce barriers to measuring colloid EFPTs. Once addressed, it is

likely that this system can be used to make EFPT measurements and draw connections between the distribution of EFPTs and properties of the underlying hidden environment.

3.5 Conclusion

While we have historically been able to describe diffusive systems and their average particles, we have only recently been able to understand the extremes and characterize their statistical behavior. In doing so, we have revealed the potential to use measurements of extreme value statistics to uncover information about the underlying, correlated environment. By measuring extreme particle location and extreme first passage times, we can determine statistical properties that describe the environment that influences the diffusing particles' behavior. We have designed, built, and tested an experimental setup that will enable future measurements of EFPTs in colloid diffusion. Preliminary results show that this setup can successfully centrifuge colloids down and subsequently image colloid movement inside the capillary tubes. Further refinement on both the data collection and analysis processes will be necessary to make complete and accurate EFPT measurements, but once available, these measurements have great potential to provide new and impactful insights into understanding the hidden environment in which particles diffuse, with applications across a wide range of systems [36, 42, 55–57, 59, 60, 93]

3.6 Supplementary Material

```
% Initialize arduino and servo control pins
a = arduino("COM5", "Mega2560");


brakePin = 'D10';
servoPin = 'D11';
runPin = 'D12';
% Position control - 16 bits
b1 = 'D22'; %b1 - most significant bit (MSB)
b2 = 'D24';
b3 = 'D26';
b4 = 'D28';
b5 = 'D30';
b6 = 'D32';
b7 = 'D34';
b8 = 'D36';
b9 = 'D23';
b10 = 'D25';
b11 = 'D27';
b12 = 'D29';
b13 = 'D31';
b14 = 'D33';
b15 = 'D35';
b16 = 'D37'; %b16 - least significant bit (LSB)
```

```
% Configure servo pins - set to output because we want to
   write info to them, rather than read data off of them
configurePin(a,brakePin,'digitalOutput') %brake
configurePin(a,servoPin,'digitalOutput') %servo
configurePin(a,runPin,'digitalOutput') %run
configurePin(a,b1,'digitalOutput') %b1 - MSB
configurePin(a,b2,'digitalOutput')
configurePin(a,b3,'digitalOutput')
configurePin(a,b4,'digitalOutput')
configurePin(a,b5,'digitalOutput')
configurePin(a,b6,'digitalOutput')
configurePin(a,b7,'digitalOutput')
configurePin(a,b8,'digitalOutput')
configurePin(a,b9,'digitalOutput')
configurePin(a,b10,'digitalOutput')
configurePin(a,b11,'digitalOutput')
configurePin(a,b12,'digitalOutput')
configurePin(a,b13,'digitalOutput')
configurePin(a,b14,'digitalOutput')
configurePin(a,b15,'digitalOutput')
configurePin(a,b16,'digitalOutput') %b16 - LSB

% Set to initial position and turn on servo
position = [0,1,1,0,1,0,1,0,1,0,1,0,0,0,0,0];
writePosition(a,position);
```

```
writeDigitalPin(a,brakePin,0);  % brake off
writeDigitalPin(a,servoPin,1);  % servo on
writeDigitalPin(a,runPin,0);    % not spinning
pause(1);
%%

% % Initialize camera
vidobj = cameraInitialization();
%%

% Create folders for file saving
t = datetime('now','Format','MM-d-y');
d = yyyymmdd(t);
name = "files-" + d;
mkdir(['data-' int2str(d) '\']);
mkdir(['data-' int2str(d) '\capillary01\']);
mkdir(['data-' int2str(d) '\capillary02\']);
mkdir(['data-' int2str(d) '\capillary03\']);
mkdir(['data-' int2str(d) '\capillary04\']);
mkdir(['data-' int2str(d) '\capillary05\']);
mkdir(['data-' int2str(d) '\capillary06\']);

%%
% Run centrifuge for set number of seconds
```

```
runTime = 2400;                    % how long to run
   centrifuge
writeDigitalPin(a,runPin,1);       % run centrifuge
pause(runTime);                    % wait 'runTime' number of
    seconds
writeDigitalPin(a,runPin,0);       % stop running centrifuge
pause(5);                          % wait for slow down
position = [0,1,1,0,1,0,1,0,1,0,1,0,0,0,0,0];
writePosition(a,position);         % preset to position 16 as
    cycle "end"

%%
% Collect test images to make sure we're good


% Store first frames in array for access in stabilization
   function
referenceFrames = {};

% set to position 16 for correct first frame
position = [0,1,1,0,1,0,1,0,1,0,1,0,0,0,0,0];
writePosition(a,position);
pause(1);

% first position: 1000 1111 0010 1100
```

```
capillaryNumber = 1;
position = [1,0,0,0,1,1,1,1,0,0,1,0,0,1,1,0];
writePosition(a,position);
pause(3);    % wait for three seconds; servo finds home
writeDigitalPin(a, brakePin, 1);
pause(1);    % wait for a second
pic = getsnapshot(vidobj);
pause(1);
writeDigitalPin(a, brakePin, 0);
referenceFrames = [referenceFrames, pic];
imwrite(pic,gray,sprintf(['data-' int2str(d) '/capillary
   %02d/frame%04d.png'],capillaryNumber,0));

% second position: 1000 1100 1011 1100
capillaryNumber = 2;
position = [1,0,0,0,1,1,0,0,1,0,1,1,1,0,1,0];
writePosition(a,position);
pause(1);    % wait for a second
writeDigitalPin(a, brakePin, 1);
pause(1);    % wait for a second
pic = getsnapshot(vidobj);
pause(1);
writeDigitalPin(a, brakePin, 0);
referenceFrames = [referenceFrames, pic];
```

```
imwrite(pic,gray,sprintf(['data-' int2str(d) '/capillary
   %02d/frame%04d.png'],capillaryNumber,0))

% third position: 1000 1010 0100 1100
capillaryNumber = 3;
position = [1,0,0,0,1,0,1,0,0,1,0,0,1,0,1,0];
writePosition(a,position);
pause(1);    % wait for a second
writeDigitalPin(a, brakePin, 1);
pause(1);    % wait for a second
pic = getsnapshot(vidobj);
pause(1);
writeDigitalPin(a, brakePin, 0);
referenceFrames = [referenceFrames, pic];
imwrite(pic,gray,sprintf(['data-' int2str(d) '/capillary
   %02d/frame%04d.png'],capillaryNumber,0))

%   repeat for remaining capillaries (to 16)
%   TO DO: rewrite into one function that takes each
   position from a list instead of repeating code block 16
    times

%%
% Set time between frames (seconds)
frametime = 240;
```

```
% set to position 16 for correct first frame
position = [0,1,1,0,1,0,1,0,1,0,1,0,0,0,0,0];
writePosition(a,position);
pause(1);

% Pass through positions, capturing and saving an image
   each time
for frameNumber=1:1999
    % first position: 1000 1111 0010 1100
    capillaryNumber = 1;
    position = [1,0,0,0,1,1,1,1,0,0,1,0,0,1,1,0];
    writePosition(a,position);
    pause(3);                           % wait for three
       seconds; servo finds home
    writeDigitalPin(a, brakePin, 1);    % brake on
    pause(1);                           % let things
       settle
    pic = getsnapshot(vidobj);          % take picture
    stablePic = imageStabilization(pic,referenceFrames,
       capillaryNumber);
    pause(1);
    writeDigitalPin(a, brakePin, 0);    % brake off, write
        image
```

```
imwrite(stablePic,sprintf(['data-' int2str(d) '/
   capillary%02d/frame%04d.png'],capillaryNumber,
   frameNumber));

% second position: 1000 1100 1011 1100
capillaryNumber = 2;
position = [1,0,0,0,1,1,0,0,1,0,1,1,1,0,1,0];
writePosition(a,position);
pause(1);    % wait for a second
writeDigitalPin(a, brakePin, 1);
pause(1);
pic = getsnapshot(vidobj);
stablePic = imageStabilization(pic,referenceFrames,
   capillaryNumber);
pause(1);
writeDigitalPin(a, brakePin, 0);
imwrite(stablePic,sprintf(['data-' int2str(d) '/
   capillary%02d/frame%04d.png'],capillaryNumber,
   frameNumber));

% third position: 1000 1010 0100 1100
capillaryNumber = 3;
position = [1,0,0,0,1,0,1,0,0,1,0,0,1,0,1,0];
writePosition(a,position);
pause(1);
```

```
    writeDigitalPin(a, brakePin, 1);
    pause(1);
    pic = getsnapshot(vidobj);
    stablePic = imageStabilization(pic,referenceFrames,
       capillaryNumber);
    pause(1);
    writeDigitalPin(a, brakePin, 0);
    imwrite(stablePic,sprintf(['data-' int2str(d) '/
       capillary%02d/frame%04d.png'],capillaryNumber,
       frameNumber));

%   repeat for remaining capillaries (to 16)
%   TO DO: rewrite into one function that takes each
   position from a list instead of repeating code block 16
    times

    pause(180)
end

%%
% close camera, clear everything
stop(vidobj)
clear a
clear vidobj
```

```
%%
function writePosition(a,b)
    writeDigitalPin(a, 'D22', b(1));
    writeDigitalPin(a, 'D24', b(2));
    writeDigitalPin(a, 'D26', b(3));
    writeDigitalPin(a, 'D28', b(4));
    writeDigitalPin(a, 'D30', b(5));
    writeDigitalPin(a, 'D32', b(6));
    writeDigitalPin(a, 'D34', b(7));
    writeDigitalPin(a, 'D36', b(8));
    writeDigitalPin(a, 'D23', b(9));
    writeDigitalPin(a, 'D25', b(10));
    writeDigitalPin(a, 'D27', b(11));
    writeDigitalPin(a, 'D29', b(12));
    writeDigitalPin(a, 'D31', b(13));
    writeDigitalPin(a, 'D33', b(14));
    writeDigitalPin(a, 'D35', b(15));
    writeDigitalPin(a, 'D37', b(16));
end

function vid = cameraInitialization
    % Initialize video - create video object, open camera
    vid = videoinput("gentl",1,"Mono8");
    triggerconfig(vid,"manual");     % allows snapshots
       whenever triggered by getsnapshot(vidobj)
```

```
    set(vid,'FramesPerTrigger',1,'Timeout',5);
    start(vid)

    % Take a test pic, display it - helps to know if the
       camera and computer are
    % communicating before running the centrifuge
    %frame = getsnapshot(vid);
    imagesc(getsnapshot(vid))  % display image
end

function stabilizedFrame = imageStabilization(
   unstableFrame,referenceFrames,capillaryNumber)
    referenceFrame = referenceFrames{capillaryNumber}(:,
       1:2001, :);
    referenceImage = im2double(referenceFrame);
    [output, Greg] = dftregistration(fft2(referenceImage),
       fft2(unstableFrame(:, 1:2001, :)),100);
    stabilizedFrame = mat2gray(abs(ifft2(Greg)));
end
```

CHAPTER IV

MEASUREMENTS OF EXTREME FIRST PASSAGE TIMES IN PHOTON TRANSPORT

4.1 Abstract

Photon transport through turbid media has typically been modeled through diffusion or telegraph equations. These models describe behavior of the average, or typical, photon with remarkable accuracy, however, we show here that they fail to capture the Extreme First Passage Times (EFPTs) of photon transport. By sending ultra-short bursts of photons through a scattering medium and timing the arrival of the first passage photon, we measure the distribution of these EFPTs of photons in a random environment. Our measured EFPTs differ from those predicted by both the diffusion approximation and telegraph equation. Instead, we observe the EFPT as the time expected for light to travel through an index-averaged medium. These results reveal flaws in both models and invite a re-examining of their underlying assumptions.

4.2 Motivation

In Chapter III, we explored the possibility of measuring extreme first passage times (EFPTs) in colloid diffusion, with the goal that the statistics of these distributions can reveal information about the shared environment through connections made in numerical work [83, 84, 157]. During my graduate work, we also sought to measure extreme first passage times in another, vastly different system: photons travelling through scattering media, which appear to also behave "diffusively". Using an ultrafast pulsed laser, we send very narrow bursts of photons into a narrow, polished-interior tube filled with silica nanosphere suspensions, making a quasi-1D scattering medium. With a single photon avalanche diode (SPAD) and time-correlated single photon counter (TCSPC), we time the first photon to pass through to the other end, down to 2ps precision. Through

power attenuation optics and built-in wavelength tuning, we can control the number of photons N in the diffusive system. By adjusting the scattering properties of the medium, particularly in varying the concentration of silica nanospheres in the suspensions, we alter the properties of the underlying environment. Utilizing a high repetition rate from the laser and a fast photon counting setup allows for collection of a large number of EFPTs in a very short amount of time. This provides a quick method for building EFPT distributions, which can then be analyzed to determine the extreme value statistics for this diffusive system.

We designed the experimental system such that different elements can be changed without affecting the path length. By using two rotating polarizers, we can attenuate the power while keeping the polarization consistent across concentrations. We flush solutions through the tube using hoses and gravity-driven flow to enable concentration changes without interfering with the setup. An XYZ translational stage keeps the SPAD mounted in place while allowing for precise repositioning without drastically increasing measurement uncertainty, particularly when neutral density filters need to be added at low scatterer concentrations to avoid oversaturating the detector. These conditions allow for measurements of EFPT with extreme (5-10ps) precision and ensure the experiment's repeatability.

This chapter reports on the relationship between scatterer concentration and the peak of the EFPT distribution, as well as the failure of the underlying random walk model in capturing the extreme behavior of photons travelling through scattering media. Additional work would be required to study the variance of these distributions to make connections to the motivating numerical work [83, 84, 157], but through the experimental work described here, we have the potential to discover new insights into the effects of the shared environment on scattering photons.

4.3 Introduction

When light passes through a scattering medium, the spatial distribution of photons is smeared out by random scattering events, resulting in a corresponding broadening of the distribution of photons from a pulsed source. This broadening has historically been modeled at short times by the telegraph equation [76–78, 159] and at asymptotically long times by the diffusion approximation [65, 66, 160]. However, these models both rely on a central assumption, that the scattering, and thus the path through the system, of each photon is independent and identically distributed. Here, we probe the quality of these models by examining a measurement of the Extreme First Passage Time (EFPT), that is, the *first* time of first arrival within a pulse of light. We use a femtosecond laser to fire pulses of light through a tunable scattering medium and measure the EFPT with a Single Photon Avalanche Diode (SPAD). We present experimental evidence that both of these models provide quantitatively and qualitatively wrong predictions for this measurement.

In this chapter, we review the history of models for the first passage of photons, then describe an experimental setup to measure photon EFPT. We describe the diffusion approximation and telegraph equation approaches to modeling photon transport, and compare EFPT predictions from these models to experimental measurements. We demonstrate that both models fail to predict the EFPT.

4.4 Background

Two widely used approximations for modeling photon transport are the diffusion approximation and the telegraph equation. The diffusion approximation predicts the bulk or average behavior of light pulses in random media and offers valuable insights into various systems across a broad range of applications [66–72]. However, the diffusion approximation fails to incorporate ballistic photons and the speed of light, making it unsuitable for short length and time scales, media with significant anisotropy or

absorption, or environments with low scattering [65, 73–76, 161]. The telegraph equation overcomes many of these limitations by accounting for the finite speed of light in a medium and capturing wave-like effects at small distances, providing a more accurate description of the bulk or typical behavior of light pulses [49, 76–82]. Discrepancies remain at distances near the source relative to the transport mean free path [76, 77, 162], and the accuracy of the predicted speed of light depends on how the scattering path length and anisotropy are treated during the derivation [82, 163, 164].

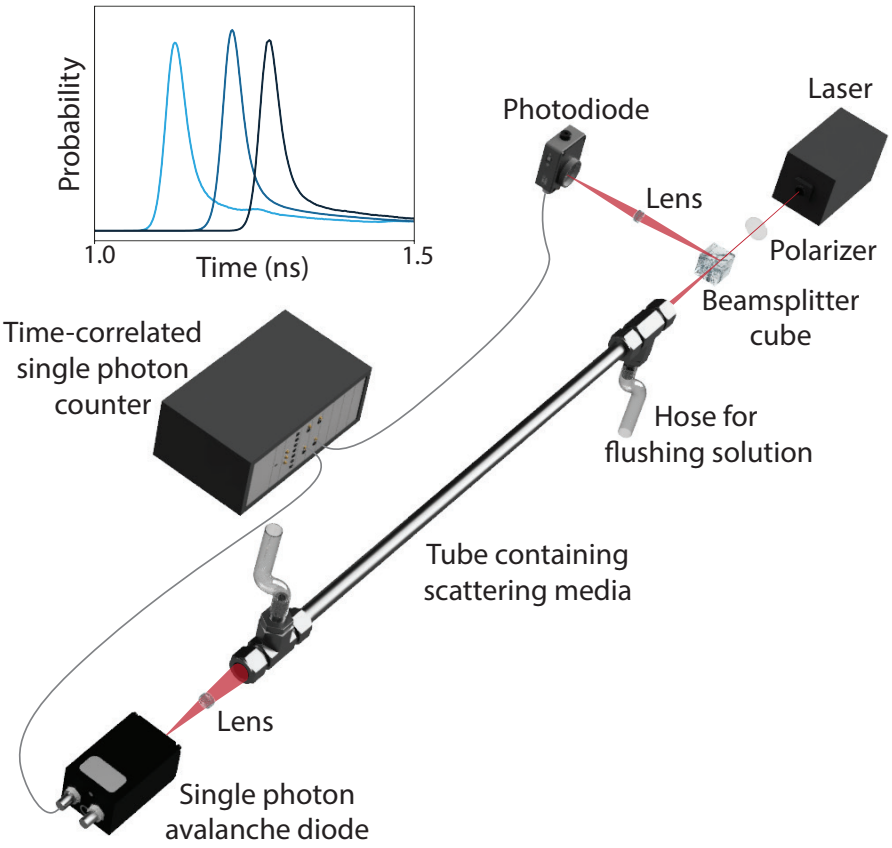


Figure 4.1. Experimental setup, consisting of elements described in the text. Signals are collected over an adjustable time period, resulting in a histogram of EFPTs. An example of such a histogram at three different concentrations of scattering media is shown, with concentration increasing from left to right, where the x axis is the time relative to the speed of light in a vacuum, and the y axis is the probability of that time as the EFPT.

First passage times have been broadly described and studied across various diffusive systems [56, 154, 165, 166], including chemical and molecular reactions [56, 59], protein interactions [60], fractal media [167], and stock market fluctuations [54, 168]. In general, extreme value distributions, which describe values drawn from the tails of a source distribution, exhibit distinct statistical behaviors [62, 64] and play a critical role in processes such as menopause timing [61], gene activation [169], and oocyte fertilization by sperm [169, 170]. In photonic systems, changes in pulse shape due to absorption and scattering have been measured [73, 74, 161, 171–174], and photon first passage time distributions have been characterized numerically and experimentally [165, 175–177]. To our knowledge, EFPT distributions have not previously been experimentally measured.

4.5 Experimental Methods

Our experimental setup is shown in Figure 4.1. Optical pulses of 140 fs in duration are generated with a femtosecond pulsed laser (Coherent Chameleon Ultra II laser) operating at central wavelengths tunable between 680-1080 nm with a repetition rate of 80 MHz and wavelength-dependent total output power range of 650-3500 mW. These pulses are sent through a power attenuating polarizer (Thorlabs GL10-B). The majority of the power is bled off through a beamsplitter (Thorlabs BS041) and sent to a photodiode (Thorlabs DET10A). This photodiode triggers a time-correlated single photon counter (TCSPC) (PicoQuant HydraHarp 400) to start a time-of-flight measurement. The remainder of the light continues into a 12.7mm diameter, 1.015 m long stainless steel tube that has been internally polished. This tube is filled with a solution of water and 20 nm diameter silica nanospheres (LUDOX AS-40). The nanospheres have an index of refraction n = 1.453-1.456, dependent on wavelength. The concentration of nanospheres is variable, in place, from volume fractions of 0 to 0.235 parts silica to 1 part water, where the maximum value is set by the volume fraction of undiluted LUDOX. The concentration

is adjusted by flushing the solution and flowing in a new solution. After traveling through the scattering medium, photons exit the tube and are concentrated through a doublet lens (Thorlabs AC254-030-B-ML) onto a Single Photon Avalanche Diode (Micro Photon Devices PDM series SPAD). The signal from the SPAD triggers the TCSPC to stop and the time of flight measurement is recorded.

The TCSPC and SPAD both have a dead-time less than 80 ns, yielding an effective experimental repetition rate of 12.5 MHz. Using a detector for the TCSPC start and stop signals allows for measurement resolution that is not limited by the dead time. Integration times varied from 1-600 s.

The SPAD detection efficiency varies with wavelength from 10-30%. From the peak laser power, approximately 3.5 W at 750 nm light, repetition rate of 80 MHz, and power attenuation from the optical components, we find a generous upper bound for the number of photons per pulse, N, entering the scattering medium as 5×10^6.

We use Ludox AS-40 as a scattering medium because it scatters strongly, absorbs minimally, is easily diluted with water, is slow to aggregate, and aggregation is easily reversed through sonication. Ludox has been well characterized for light scattering purposes [178–180]. The small size of the silica nanospheres (roughly 3% of the wavelengths used in these experiments) places us firmly within the Rayleigh scattering regime for which we can calculate σ_s and μ_s, the scattering cross section and coefficient, as [68, 160]

$$\sigma_s = \frac{2\pi^5}{3}\frac{d^6}{\lambda^4}\left(\frac{n_{silica}^2 - n_{water}^2}{n_{silica}^2 + 2n_{water}^2}\right)^2, \ \mu_s = \frac{C}{\frac{4}{3}\pi\left(\frac{d}{2}\right)^3}\sigma_s \tag{4.1}$$

where d is the scatterer diameter, λ is the wavelength of light being scattered, n is the refractive index of the scatterer material, C is the volume concentration of scatterers, and the scattering coefficient is the inverse of the scattering path length with units $\frac{1}{\mathrm{m}}$. Using measurements performed with a UV/Vis/NIR spectrophotometer (Perkin Elmer Lambda-

1050), we further characterize this medium by measuring σ_a, the absorption cross section, and use the Beer-Lambert law to find μ_a, the absorption coefficient, as [181]

$$\sigma_a = 1.53 \times 10^{-22} \text{ m}^2, \ \mu_a = \frac{C}{\frac{4}{3}\pi\left(\frac{d}{2}\right)^3}\sigma_a. \tag{4.2}$$

4.6 Models for Photon Transport

A classical approximation to the spatial and temporal distribution of photons is the equation of transfer [65, 66]. As there is currently no general solution to this time-dependent radiative transfer equation, most applications rely on approximations to derive a more tractable solution. Different approximation methods yield distinct solutions, with the diffusion approximation and the telegraph equation being two widely used approaches. In the following, we approximate the transmission of light through a slender tube filled with scattering medium as a one-dimensional process. We describe these two approaches below, resulting in two distinct photon probability distributions. From the probability distribution of photon locations, we derive an approximation for the extreme first passage time (EFPT) past a distance L. We approximate this as the first time at which the cumulative probability beyond L surpasses $1/N$, for N incident photons [84].

4.6.1 The equation of transfer. The equation of transfer is given by [65, 66],

$$\begin{aligned}\frac{1}{c}\partial_t L(\mathbf{r},\hat{s},t) + \nabla\cdot L(\mathbf{r},\hat{s},t)\,\hat{s} &= -(\mu_s+\mu_a)\,L(\mathbf{r},\hat{s},t) \\ &+ \mu_s\int\int_{4\pi} L\left(\mathbf{r},\hat{s'},t\right) f\left(\hat{s}\cdot\hat{s'}\right) d\Omega' + S(\mathbf{r},\hat{s},t)\,.\end{aligned} \tag{4.3}$$

This equation determines the rate of change of the radiance, L, through position $\mathbf{r}$, in direction $\hat{s}$, and at time t. The radiance originates at a source, described by S, and is lost to the absorption coefficient, μ_a, and scattered by the scattering coefficient, μ_s. The speed of light in the medium is c, and $f(\hat{s}\cdot\hat{s'})$ is the normalized differential scattering probability for photons traveling in a direction $\hat{s'}$ to scatter into the direction $\hat{s}$.

(4.3) can be integrated over all solid angles to find a continuity equation governed by the photon density, $\varphi(\mathbf{r},t)$, and photon flux, $\mathbf{j}(\mathbf{r},t)$ [66]. When considering scattering in a long tube it is useful to approximate the system as quasi-one-dimensional. Because $f(\hat{s}\cdot\hat{s}')$ can be thought of as a distribution of scattering angles where $\cos\theta = \hat{s}\cdot\hat{s}'$, it will reduce to a single parameter, $\langle\cos\theta\rangle$, when integrated over all angles. For Rayleigh scattering, which is isotropic in both forward and backward directions [160], $\langle\cos\theta\rangle = 0$.

4.6.2 Diffusion approximation. When the total volume concentration of scatterers greatly exceeds 1%, (4.3) can be estimated by a diffusion approximation. Under the assumption that photons interact with many particles, we assume a nearly uniform angular scattering distribution [65, 160]. By expressing the radiance $L(\mathbf{r},t)$ as the sum of an isotropic photon density $\varphi(\mathbf{r},t)$ and a small directional flux, neglecting variations and anisotropy in the source term $S(\mathbf{r},t)$, integrating over all solid angles, and approximating as a one-dimensional system, we obtain [66]

$$D\partial_r^2\varphi(r,t) - \mu_a c\varphi(r,t) = \partial_t\varphi(r,t) - cS(r,t), \tag{4.4}$$

with diffusion coefficient

$$D = \frac{c}{3(\mu_s+\mu_a)}. \tag{4.5}$$

The solution to (4.4) is well-established as a Gaussian multiplied by a decaying exponential term that accounts for absorption [66].

Under this diffusion approximation photons move as Brownian walkers in a semi-infinite medium, starting at the origin and whose position we denote as $B(t)$. When absorption is minimal, the probability of a photon to be found beyond a distance L at time t is [56, 62]

$$P(B(t)\geq L) = 1 - \mathrm{erf}\left(\frac{L}{2\sqrt{Dt}}\right). \tag{4.6}$$

We approximate the expected value of the EFPT as the time at which this probability surpasses $1/N$. We note that at short times the diffusion approximation yields non-physical behavior because the maximum photon speed in this approximation is unbounded.

4.6.3 Telegraph equation. The telegraph equation offers a more accurate model for photon transport, incorporating the ballistic motion of photons. By using asymptotic expansions to approximate a solution to (4.3) [163, 164, 182], accounting for the movement of photons in and out of each direction as opposing "streams" [77, 79, 80, 183], or by various other methods of derivation [78, 81, 162, 165, 184], we arrive at a telegraph equation for photon transport [77], which governs the evolution of φ as

$$\begin{aligned}\partial_r^2 \varphi(r,t) =& \frac{1}{c^2}\partial_t^2 \varphi(r,t) + \frac{1}{c}(2\mu_a + 3\mu_s)\,\partial_t \varphi(r,t) \\ &+ \mu_a(\mu_a + 3\mu_s)\,\varphi. \end{aligned} \tag{4.7}$$

At short times, (4.7) reduces to the wave equation. At long times and in the limit of μ_a going to zero we recover (4.4), the standard diffusion approximation, with diffusion coefficient [77]

$$D = \frac{c}{3\mu_s}. \tag{4.8}$$

The general solution to this telegraph equation is given by [76, 78]

$$\begin{aligned}\varphi(r,t) = \frac{1}{2}e^{-(\mu_a c+\gamma)t}\Bigg[&\delta(ct-r) + \delta(ct+r) \\ &+ \Theta(ct-|r|)\left(\frac{\gamma}{c}I_0\left(\frac{\gamma u}{c}\right) + \frac{\gamma t}{u}I_1\left(\frac{\gamma u}{c}\right)\right)\Bigg] \end{aligned} \tag{4.9}$$

where δ is the Dirac delta function, Θ is the Heaviside step function, I_0 and I_1 are modified Bessel functions of the first kind, $u = \sqrt{c^2t^2 - r^2}$ represents the position relative to that of a ballistic photon, and $\gamma = \frac{3}{2}c\mu_s$ is a characteristic time scale for scattering events [78, 81, 185, 186]. We solve this numerically to obtain EFPT predictions.

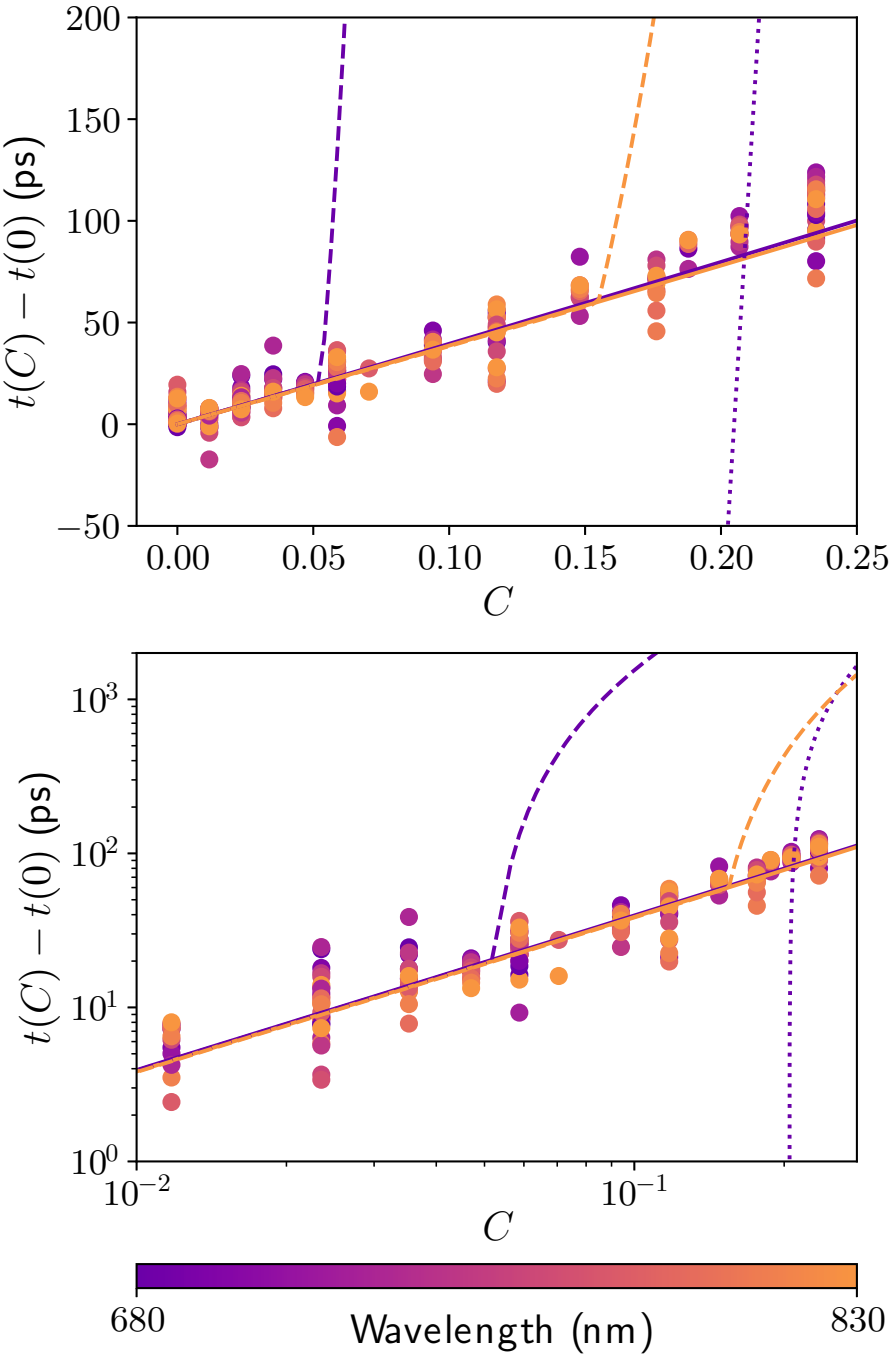


Figure 4.2. EFPT differences measured experimentally, in picoseconds, versus volume concentration C. Both plots are the same, with different scales. Solid lines are predicted EFPTs for a photon traveling through an index-averaged medium of silica and water. Experimental values are shown as points, telegraph equation predictions are shown as dashed lines, and the diffusion approximation is shown as dotted lines. Color indicates wavelength from 680 nm (violet) to 830 nm (orange). Predictions were made using $N = 5 \times 10^6$ photons. The orange dotted line does not appear in this figure as the values fail to cross over the measured range.

4.7 Results and Discussion

Figure 4.2 shows $t(C)$, the time of the peak of the EFPT distribution for scatterer volume concentration C, for a range of wavelengths and volume concentrations. For each wavelength measured, this time is shown relative to $t(0)$, the time of the peak of the EFPT distribution for pure water recorded at that wavelength. The measured EFPTs show no wavelength dependence and increase linearly with C, reaching approximately 100 ps for $C = 0.235$. The measured EFPT differences are consistent with the extreme photons traveling at the speed of light through a *non-scattering* index-averaged medium at each concentration.

The predictions of the two models are plotted as dotted lines (diffusion approximation) and dashed lines (telegraph equation) for wavelengths at the extreme ends of our experimental range. These predictions are calculated using $N \simeq 5 \times 10^6$. Because the EFPT increases with decreasing N [62], this upper limit for N provides a lower bound on the predicted values of the peak EFPT. Additionally, the relative difference between the predictions at 680 nm and 830 nm becomes larger as N decreases. The diffusion approximation predicts non-physical results for small concentrations, allowing photons to travel faster than the speed of light for C below approximately 0.21 at 680 nm and at all concentrations for 830 nm. At higher concentrations, the diffusion approximation predicts increasing EFPT differences for 680 nm, exceeding 650 ps (680 nm) at $C = 0.235$. Relatively speaking, the telegraph equation does a better job and predicts a linear relationship for EFPT delay at low concentrations, determined by the speed of light in the index-averaged medium. However, for concentrations beyond approximately 0.05 (680 nm) and 0.15 (830 nm), scattering and absorption cause the EFPT difference to increase rapidly and deviate from the measured values. Maximum predicted delays of 8,000 ps (680 nm) and 900 ps (830 nm) occur at $C = 0.235$.

4.8 Conclusion

The diffusion and telegraph approximations fail to accurately describe EFPT photons, either violating causality (diffusion) or predicting unrealistically large EFPT differences (diffusion and telegraph). In order to provide accurate predictions, the telegraph equation would require either unphysically large photon counts of $N \gtrapprox 10^{16}$, far exceeding the laser output to achieve wavelength-independent results, or an anisotropy factor ($\langle \cos\theta \rangle \geq 0.4$) that contradicts the isotropic-scattering behavior of Rayleigh scattering. While these models are effective at predicting the behavior of the average photon in scattering media and can be used to infer bulk properties, they fail to describe extreme photons. These results suggest that assumptions made in the underlying random walk approach are incorrect. Near-field effects present at high scatterer number density and the breakdown of self-similarity in photon transport could provide a route toward explaining why EFPTs follow the index-averaged predictions long after increased scattering should have increased delays, as these effects can produce photon trajectories that favor forward-scattering [187–190]. Alternatively, a model based on random walks which incorporate correlated or even quantum mechanical behavior may produce more accurate predictions and could better describe the underlying physical process. Such a model would unlock the potential for photon EFPT statistics to uncover critical insights about the diffusive environment, with broad applications across many areas of science [54, 56, 59–62, 165–170].

4.9 Acknowledgments

We thank M. Allgaier, J. Hass, D. Allcock, I. Corwin, and R. Parthasarathy for discussions. This work was funded by the W. M. Keck Foundation Science and Engineering grant on “Extreme Diffusion”.

CHAPTER V

CONCLUSION

The work presented in this dissertation sheds new light on how the traditional Einstein random walk model, where each particle in a diffusing system takes independent and random steps through time, fails to capture the full picture of diffusion. While this model works well enough in describing the average particle's behavior and statistics that we can make accurate predictions and discover new insights into diffusive systems across a wide range of disciplines, the model fails in accurately describing the behavior of extreme particles. A new model is needed to describe these particles, that factors in correlations from the shared environment. From such a model, we can then make accurate predictions of these extreme particles and gain new insights into the underlying environment. The work presented in this dissertation explored a random walk in a Beta-distributed random environment and its connection to the KPZ universality class, proposed an experimental method for measuring extreme first passage times in diffusing colloids, and detailed an experiment that revealed the failure of independent-random-walk-based models for photon propagation. This work demonstrates the failure of the traditional Einstein random walk for outlier particles, and highlights the importance of factoring correlations into the theoretical models we use to describe real diffusive systems.

In Chapter II, we built on existing literature on extreme particle locations which propose a connection between large deviations for times of order $\log(N)$ and the KPZ universality class [129, 130, 133], as well as a phase transition around times of $(\log(N))^2$ [53]. A mathematical framework for a random walk in a random environment, where a one-dimensional system of particles undergo a random walk on a spatially and

temporally variant random biasing field with biases drawn from a Beta distribution, had been proposed, and predicted a Tracy-Widom distribution for walker positions.

To determine what is measured in a system of particles diffusing in the aforementioned biased environment, Jacob Hass and I ran simulations of diffusing particles from system sizes of $N = 10^2$ to $N = 10^{300}$, and this work is described in Chapter II. We evolved the particle location probability distribution function for these systems according to this biased walk, and measured the extreme (furthest) particle locations throughout time. By studying the variance of these extreme particle locations, we found the anticipated Tracy-Widom dynamics and uncovered a new phase with fluctuations tied to the KPZ universality class. A key result of this work is that the environmental variance of a physical system can be indirectly measured by determining the variance in the extreme particle location, then subtracting off the sample variance. In doing so, the underlying environment of this physical system can be better understood, and new insights into diffusion in real systems revealed.

Because we know from Chapter II (and further work done by Hass et al [84]) that we can learn about the shared environment of diffusing particles through the extreme value statistics, there is an opportunity to measure these statistics in a real physical system to learn about the underlying environment. Through such measurements, we can confirm whether diffusive systems are well represented by either the traditional uncorrelated Einstein model or the correlated random walk proposed in this earlier work.

In Chapter III, I developed an experimental apparatus to gather first passage times of colloids diffusing through water. This will allow future researchers to explore the first passage time statistics and uncover properties of the underlying environment in which these particles diffuse. I built a centrifuge that doubles as a microscope stage, isolating colloids to one end of a glass capillary tube, and tracking the first particle to enter and

cross the microscope's field of view. While work remains to be done on ensuring that all colloids are truly isolated and that no flow is present in the capillaries, as well as in processing the images and tracking particle trajectories, preliminary results are promising. Once these issues are resolved, we should be able to collect first passage times and measure the variance, particularly as experimental parameters are changed, and determine what scaling regimes exist.

Photon transport has been well modelled by the Boltzmann Radiative Transfer Equation, but it's computationally intensive and, to our knowledge, has yet to be solved analytically. As a result, approximations to the equation are made in order to make predictions for photon propagation and gather information about photonic systems. Assuming a lot of scatterers and minimal absorption, as well as long overall distances, we can approximate with a diffusion or telegraph equation. These models work quite well to predict the average photon behavior, as exhibited by how the models are used to measure optical parameters in a wide variety of applications. However, these models rely on the assumption that photon scattering is completely independent and totally elastic. Again, by neglecting correlated movement due to quantum mechanics and/or optical interference, we predict that these models fail the extremes.

In Chapter IV, I measured photon extreme first passage times in random media of varying scatterer concentrations. From these measurements, I determined that the traditional diffusion approximation and telegraph equation fail to describe these extremes. Instead, the extreme photons travel as though they do not scatter at all, "seeing" an index-averaged medium well beyond the point where scatterer concentration are expected to delay the extreme first passage time. This shows that these models do not accurately capture the underlying physics, and a better model that factors in quantum mechanical or near-field effects is needed to more accurately describe extreme first

passage photons [187, 189]. With a more precise model, we can better characterize the scattering environment photons travel through, with broad applications across scientific research [70–72, 160].

Measuring how the variance of the photon extreme first passage time distribution changes with scatterer concentration and laser power could connect this work to that of Chapter II and III, particularly in determining if environmental properties can be extracted from these measurements. Additionally, changing the scattering medium, expanding the wavelength range in the experiment, varying polarization, and otherwise introducing new changing variables could provide further insight into the underlying physical phenomena. Numerically modelling the full pulse propagation, modelling diffusing photons as in Chapter II, or using Monte Carlo methods to work with the full Boltzmann Radiative Transfer Equation could all be fascinating ways to connect experimental data to theoretical models and numerical predictions beyond the two approximations explored in this work.

REFERENCES CITED

[1] T. L. Carus,
On the Nature of Things (Richer Resources Publications, 2010).

[2] F. Bacon, *Novum Organum; Or, True Suggestions for the Interpretation of Nature*, edited by J. Devey (P. F. COLLIER & SON, New York, 1902).

[3] R. Boyle, *New experiments physico-mechanicall, touching the spring of the air, and its effects (made, for the most part, in a new pneumatical engine): written by way of letter to the Right Honorable Charles, Lord Vicount of Dungarvan, eldest son to the Earl of Corke* (Printed by H. Hall ... for Tho. Robinson, Oxford, 1660).

[4] E. Halley, *An Historical Account of the Trade Winds, and Monsoons, Observable in the Seas between and Near the Tropicks, with an Attempt to Assign the Phisical Cause of the Said Winds, By E. Halley*, Philosophical transactions (Royal Society (Great Britain) : 1683) **16**, 153–168 (1686), publisher: The Royal Society.

[5] Newton, *VII. Scala graduum caloris*, Philosophical Transactions of the Royal Society of London **22**, 824–829 (1997), publisher: Royal Society.

[6] G.- L. T. d. B. .-. . m. A. d. t. Du Châtelet, *Dissertation sur la nature et la propagation du feu* (Prault fils, Paris, 1744).

[7] D. Bernoulli, *Hydrodynamica, sive de viribus et motibus fluidorum commentarii : opus academicum ab auctore, dum Petropoli ageret, congestum* (1738).

[8] M. V. Lomonosov, *Mikhail Vasil'evich Lomonosov on the Corpuscular Theory* (Harvard University Press, 1970).

[9] Sadi Carnot, *Réflexions sur la puissance motrice du feu et sur les machines propres à développer atte puissance* (Bachelier Libraire, Paris, 1824).

[10] in *Mathematical and Physical Papers*, Transactions of The Royal Society of Edinburgh, Vol. 20, edited by W. Thomson (Royal Society of Edinburgh, 1851) pp. 174–332.

[11] Rudolf Clausius, *The Mechanical Theory of Heat: With Its Applications to the Steam-engine and to the Physical Properties of Bodies* (J. Van Voorst, London, 1867).

[12] J.-B.-J. Fourier, *The analytical theory of heat* (At the University Press, Cambridge, 1878).

[13] J. C. Maxwell and J. W. S. Rayleigh, *Theory of heat* (London, New York [etc.] Longmans, Green, 1908).

[14] J. P. Joule, *The Scientific Papers of James Prescott Joule*, Cambridge Library Collection - Physical Sciences, Vol. 1 (Cambridge University Press, Cambridge, 2011).

[15] L. Boltzmann, *Weitere Studien über das Warmegleichgewicht unter Gasmolekülen (Further Studies on the Thermal Equilibrium of Gas Molecules, The Kinetic Theory of Gases)*, Sitzungsberichte der Kaiserlichen Akademie der Wissenschaften **66**, 275–370 (1872).

[16] C.-L. Navier, *Mémoire sur les lois du Mouvement des Fluides*, Mémoires de l'Académie Royale des Sciences de l'Institut de France **6**, 389–440 (1827).

[17] G. G. Stokes, *On the Effect of the Internal Friction of Fluids on the Motion of Pendulums*, Transactions of the Cambridge Philosophical Society **9**, 8 (1851), aDS Bibcode: 1851TCaPS...9....8S.

[18] T. Graham, *XXVII. On the law of the diffusion of gases*, The London, Edinburgh, and Dublin Philosophical Magazine and Journal of Science **2**, 175–190 (1833), publisher: Taylor & Francis _eprint: https://doi.org/10.1080/14786443308648004.

[19] A. Fick, *V. On liquid diffusion*, The London, Edinburgh, and Dublin Philosophical Magazine and Journal of Science **10**, 30–39 (1855).

[20] J. Ingenhousz, *New Experiments and Observations on Diverse Physical Objects*, T. Barrois le jeune, Paris (1785).

[21] R. Brown, *XXVII. A brief account of microscopical observations made in the months of June, July and August 1827, on the particles contained in the pollen of plants; and on the general existence of active molecules in organic and inorganic bodies*, The Philosophical Magazine **4**, 161–173 (1828).

[22] R. Brown, *XXIV. Additional remarks on active molecules*, The Philosophical Magazine **6**, 161–166 (1829).

[23] P. W. van der Pas, *The Discovery of the Brownian Motion*, Scientiarum Historia: Journal of the History of Science and Medicine **13**, 27–35 (1971).

[24] J. Regnault, *Calcul des chances et philosophie de la bourse* (Paris : Mallet-Bachelier [et] Castel, 1863).

[25] L. Bachelier, *Théorie de la spéculation*, Annales scientifiques de l'École Normale Supérieure **17** (1900).

[26] A. Einstein, *Über die von der molekularkinetischen Theorie der Wärme geforderte Bewegung von in ruhenden Flüssigkeiten suspendierten Teilchen*, Annalen der Physik **322**, 549–560 (1905).

[27] W. Sutherland, *LXXV. A dynamical theory of diffusion for non-electrolytes and the molecular mass of albumin*, The London, Edinburgh, and Dublin Philosophical Magazine and Journal of Science **9**, 781–785 (1905).

[28] M. von Smoluchowski, *Zur kinetischen Theorie der Brownschen Molekularbewegung und der Suspensionen*, Annalen der Physik **326**, 756–780 (1906).

[29] J. B. Perrin, *Le Mouvement Brownien et la Réalité Moleculaire*, Ann. Chimi. Phys. **18**, 5–114 (1909).

[30] C. Cruickshank Miller, *The Stokes-Einstein Law for Diffusion in Solution on JSTOR*, Proceedings of the Royal Society of London A, **106**, 724–749 (1924).

[31] P. H. Kao and R. J. Yang, *Virus Diffusion in Isolation Rooms*, Journal of Hospital Infection **62**, 338–345 (2006).

[32] D. Le Bihan, E. Breton, D. Lallemand, P. Grenier, E. Cabanis, and M. Laval-Jeantet, *MR imaging of intravoxel incoherent motions: application to diffusion and perfusion in neurologic disorders.*, Radiology **161**, 401–407 (1986), publisher: Radiological Society of North America.

[33] D. Le Bihan, *Diffusion MRI: what water tells us about the brain*, EMBO Molecular Medicine **6**, 569–573 (2014), publisher: John Wiley & Sons, Ltd.

[34] A. A. K. Abdel Razek, M. Thabet, and E. A. Salam, *Apparent Diffusion Coefficient of the Placenta and Fetal Organs in Intrauterine Growth Restriction*, Journal of Computer Assisted Tomography **43**, 507–512 (2019).

[35] E. Syková and C. Nicholson, *Diffusion in Brain Extracellular Space*, Physiological Reviews **88**, 1277–1340 (2008).

[36] C. Nicholson and E. Syková, *Extracellular space structure revealed by diffusion analysis*, Trends in Neurosciences **21**, 207–215 (1998).

[37] C. Nicholson, *Diffusion and Related Transport Mechanisms in Brain Tissue*, Reports on Progress in Physics **64**, 815–884 (2001), publisher: IOP Publishing.

[38] C. A. C. Wijman, M. Mlynash, A. F. Caulfield, A. W. Hsia, I. Eyngorn, R. Bammer, N. Fischbein, G. W. Albers, and M. Moseley, *Prognostic value of brain diffusion-weighted imaging after cardiac arrest*, Annals of Neurology **65**, 394–402 (2009).

[39] W. Feller, *Diffusion Processes in Genetics*, Proceedings of the Second Berkeley Symposium on Mathematical Statistics and Probability **2**, 227–247 (1951), publisher: University of California Press.

[40] J. Wakeley, *The Limits of Theoretical Population Genetics*, Genetics **169**, 1–7 (2005).

[41] W. J. Ewens, *Mathematical Population Genetics, I. Theoretical Introduction*, Vol. 27 (2012).

[42] D. Waxman, *The Diffusion Equation of Random Genetic Drift– Biology's Analogue of the Schrödinger Equation?*, Contemporary Physics **58**, 253–261 (2017).

[43] K. Kanazawa, T. G. Sano, A. Cairoli, and A. Baule, *Loopy Lévy flights enhance tracer diffusion in active suspensions*, Nature **579**, 364–367 (2020), number: 7799 Publisher: Nature Publishing Group.

[44] S. Ramaswamy, *The Mechanics and Statistics of Active Matter*, Annual Review of Condensed Matter Physics **1**, 323–345 (2010), _eprint: https://doi.org/10.1146/annurev-conmatphys-070909-104101.

[45] S. K. Ghosh, A. G. Cherstvy, and R. Metzler, *Non-Universal Tracer Diffusion in Crowded Media of Non-Inert Obstacles*, Physical Chemistry Chemical Physics **17**, 1847–1858 (2015).

[46] B. Wang, J. Kuo, S. C. Bae, and S. Granick, *When Brownian diffusion is not Gaussian*, Nature Materials **11**, 481–485 (2012).

[47] J. P. Bouchaud and A. Georges, *Anomalous diffusion in disordered media: Statistical mechanisms, models and physical applications*, Physics Reports **195**, 127–293 (1990).

[48] R. Metzler, *Brownian motion and beyond: first-passage, power spectrum, non-Gaussianity, and anomalous diffusion*, Journal of Statistical Mechanics: Theory and Experiment **2019**, 114003–114003 (2019).

[49] A. K. Das, *Some Non-Fickian Diffusion Equations: Theory and Applications*, Defect and Diffusion Forum **162-163**, 97–118 (1998), publisher: Trans Tech Publications Ltd.

[50] H. G. E. Hentschel and I. Procaccia, *Relative Diffusion in Turbulent Media: The Fractal Dimension of Clouds*, Physical Review A **29**, 1461–1470 (1984), publisher: American Physical Society.

[51] S. Condamin, O. Bénichou, V. Tejedor, R. Voituriez, and J. Klafter, *First-passage times in complex scale-invariant media*, Nature **450**, 77–80 (2007), publisher: Nature Publishing Group.

[52] G. Barraquand and I. Corwin, *Random-walk in Beta-distributed random environment*, Probability Theory and Related Fields **167**, 1057–1116 (2017).

[53] P. Le Doussal and T. Thiery, *Diffusion in time-dependent random media and the Kardar-Parisi-Zhang equation*, Physical Review E **96**, 010102–010102 (2017).

[54] L. Barney and G. H. Gunaratne, *First-Passage-Time Distribution for Variable-Diffusion Processes*, Journal of Statistical Physics **167**, 878–891 (2017).

[55] H. Liu, C.-Y. Liao, J.-Y. Ko, and J.-S. Lih, *Anchoring effect on first passage process in Taiwan financial market*, Physica A: Statistical Mechanics and its Applications **477**, 114–127 (2017).

[56] S. Redner, *A Guide to First-Passage Processes* (Cambridge University Press, Cambridge, 2001).

[57] S. Iyer-Biswas and A. Zilman, *First Passage processes in cellular biology*, Advances in Chemical Physics **160**, 261–306 (2015).

[58] D. S. Grebenkov and J.-F. Rupprecht, *The escape problem for mortal walkers*, The Journal of Chemical Physics **146**, 084106 (2017).

[59] D. S. Grebenkov, R. Metzler, and G. Oshanin, *A molecular relay race: sequential first-passage events to the terminal reaction centre in a cascade of diffusion controlled processes*, New Journal of Physics **23**, 093004 (2021), publisher: IOP Publishing.

[60] N. F. Polizzi, M. J. Therien, and D. N. Beratan, *Mean First-Passage Times in Biology*, Israel Journal of Chemistry **56**, 816–824 (2016).

[61] S. D. Lawley and J. Johnson, *Slowest first passage times, redundancy, and menopause timing*, Journal of Mathematical Biology **86**, 90 (2023).

[62] S. D. Lawley, *Distribution of extreme first passage times of diffusion*, Journal of Mathematical Biology **80**, 2301–2325 (2020).

[63] S. D. Lawley and J. B. Madrid, *A Probabilistic Approach to Extreme Statistics of Brownian Escape Times in Dimensions 1, 2, and 3*, Journal of Nonlinear Science **30**, 1207–1227 (2020).

[64] S. D. Lawley, *Universal formula for extreme first passage statistics of diffusion*, Physical Review E **101**, 012413 (2020), publisher: American Physical Society.

[65] A. Ishimaru, *Wave Propagation and Scattering in Random Media* (1997).

[66] R. C. Haskell, L. O. Svaasand, T. T. Tsay, T. C. Feng, M. S. McAdams, and B. J. Tromberg, *Boundary conditions for the diffusion equation in radiative transfer*, Journal of the Optical Society of America. A, Optics, Image Science, and Vision **11**, 2727–2741 (1994).

[67] S. Chandrasekhar, *Stochastic Problems in Physics and Astronomy*, Reviews of Modern Physics **15**, 1–89 (1943), publisher: American Physical Society.

[68] S. Chandrasekhar, *Radiative Transfer*, The International Series of Monographs on Physics (Oxford, Clarendon Press, London, 1950).

[69] J. C. Brown, P. N. Pusey, J. W. Goodwin, and R. H. Ottewill, *Light scattering study of dynamic and time-averaged correlations in dispersions of charged particles*, Journal of Physics A: Mathematical and General **8**, 664–682 (1975).

[70] M. Allgaier and B. J. Smith, *Diffuse optics for glaciology*, Optics Express **29**, 18845–18864 (2021), publisher: Optica Publishing Group.

[71] H. Taitelbaum, in *Anomalous Diffusion From Basics to Applications*, Lecture Notes in Physics, Vol. 519, edited by A. Pękalski and K. Sznajd-Weron (Springer, Berlin, Heidelberg, 1999) pp. 160–174.

[72] C. Amendola, L. Spinelli, D. Contini, A. D. Carli, C. Martinelli, M. Fumagalli, and A. Torricelli, *Accuracy of homogeneous models for photon diffusion in estimating neonatal cerebral hemodynamics by TD-NIRS*, Biomedical Optics Express **12**, 1905–1921 (2021), publisher: Optica Publishing Group.

[73] K. M. Yoo, F. Liu, and R. R. Alfano, *When does the diffusion approximation fail to describe photon transport in random media?*, Physical Review Letters **64**, 2647–2650 (1990), publisher: American Physical Society.

[74] X. Zhang and Z.-Q. Zhang, *Wave transport through thin slabs of random media with internal reflection: Ballistic to diffusive transition*, Physical Review E **66**, 016612 (2002), publisher: American Physical Society.

[75] R. Pierrat, J.-J. Greffet, and R. Carminati, *Photon diffusion coefficient in scattering and absorbing media*, JOSA A **23**, 1106–1110 (2006), publisher: Optica Publishing Group.

[76] D. J. Durian and J. Rudnick, *Photon migration at short times and distances and in cases of strong absorption*, JOSA A **14**, 235–245 (1997), publisher: Optica Publishing Group.

[77] P.-A. Lemieux, M. U. Vera, and D. J. Durian, *Diffusing-light spectroscopies beyond the diffusion limit: The role of ballistic transport and anisotropic scattering*, Physical Review E **57**, 4498–4515 (1998), publisher: American Physical Society.

[78] S. Goldstein, *On Diffusion by Discontinuous Movements, and on the Telegraph Equation*, The Quarterly Journal of Mechanics and Applied Mathematics **4**, 129–156 (1951).

[79] D. J. Durian, *Two-stream theory of diffusing light spectroscopies*, Physica A: Statistical Mechanics and its Applications **229**, 218–235 (1996).

[80] J. Masoliver, J. M. Porrà, and G. H. Weiss, *Solutions of the telegrapher's equation in the presence of traps*, Physical Review A **45**, 2222–2227 (1992), publisher: American Physical Society.

[81] J. Masoliver and G. H. Weiss, *Finite-velocity diffusion*, European Journal of Physics **17**, 190 (1996).

[82] A. Y. Polishchuk, S. Gutman, M. Lax, and R. R. Alfano, *Photon-density modes beyond the diffusion approximation: scalar wave-diffusion equation*, JOSA A **14**, 230–234 (1997), publisher: Optica Publishing Group.

[83] J. B. Hass, A. N. Carroll-Godfrey, I. Corwin, and E. I. Corwin, *Anomalous fluctuations of extremes in many-particle diffusion*, Physical Review E **107**, L022101 (2023), publisher: American Physical Society.

[84] J. B. Hass, I. Corwin, and E. I. Corwin, *First-passage time for many-particle diffusion in space-time random environments*, Physical Review E **109**, 054101 (2024), publisher: American Physical Society.

[85] A. N. Carroll-Godfrey and E. I. Corwin, Measurements of extreme first passage times in photon transport (2025), arXiv:2502.19359 [physics].

[86] M. J. Saxton and K. Jacobson, *Single-Particle Tracking: Applications to Membrane Dynamics*, Annual Review of Biophysics and Biomolecular Structure **26**, 373–399 (1997).

[87] P. A. Pinto and R. G. Eastman, *The Physics of Type Ia Supernova Light Curves. II. Opacity and Diffusion*, The Astrophysical Journal **530**, 757–776 (2000).

[88] F. Höfling and T. Franosch, *Anomalous Transport in the Crowded World of Biological Cells*, Reports on Progress in Physics **76**, 10.1088/0034-4885/76/4/046602 (2013).

[89] C. Manzo and M. F. Garcia-Parajo, *A Review of Progress in Single Particle Tracking: From Methods to Biophysical Insights*, Reports on Progress in Physics **78**, 10.1088/0034-4885/78/12/124601 (2015).

[90] R. Metzler, J.-H. Jeon, and A. G. Cherstvy, *Non-Brownian Diffusion in Lipid Membranes: Experiments and Simulations*, Biochimica Et Biophysica Acta **1858**, 2451–2467 (2016).

[91] H. Shen, L. J. Tauzin, R. Baiyasi, W. Wang, N. Moringo, B. Shuang, and C. F. Landes, *Single Particle Tracking: From Theory to Biophysical Applications*, Chemical Reviews **117**, 7331–7376 (2017).

[92] L. Hufnagel, D. Brockmann, and T. Geisel, *Forecast and control of epidemics in a globalized world*, Proceedings of the National Academy of Sciences **101**, 15124–15129 (2004), publisher: National Academy of Sciences Section: Biological Sciences.

[93] R. Metzler, G. Oshanin, and S. Redner, *First-passage phenomena and their applications* (World Scientific Publishing Co., 2014).

[94] A. Einstein, *Zur Theorie Der Brownschen Bewegung*, Annalen der Physik **324**, 371–381 (1906).

[95] A. Einstein, *Theoretische Bemerkungen Über Die Brownsche Bewegung*, Zeitschrift für Elektrochemie und angewandte physikalische Chemie **13**, 41–42 (1907).

[96] F. Rassoul-Agha, T. Seppäläinen, and A. Yilmaz, *Quenched Free Energy and Large Deviations for Random Walks in Random Potentials*, Communications on Pure and Applied Mathematics **66**, 202–244 (2013).

[97] P. Langevin, *Sur La Theorie Du Mouvement Brownien*, Compt. Rendus **146**, 530–533 (1908).

[98] W. Sutherland, *LII. The Viscosity of Gases and Molecular Force*, The London, Edinburgh, and Dublin Philosophical Magazine and Journal of Science **36**, 507–531 (1893), publisher: Taylor & Francis.

[99] M. Von Smoluchowski, *Notiz Uiber Die Berechnung Der Brownschen Molekularbewegung Bei Der Ehrenhaft-Millikanschen Versuchsanordning*, Phys. Z **16**, 318–321 (1915).

[100] J. Perrin, *Mouvement brownien et molécules*, Journal de Chimie Physique **8**, 57–91 (1910), publisher: EDP Sciences.

[101] G. E. Uhlenbeck and L. S. Ornstein, *On the Theory of the Brownian Motion*, Physical Review **36**, 823–841 (1930), publisher: American Physical Society.

[102] R. Huang, I. Chavez, K. M. Taute, B. Lukić, S. Jeney, M. G. Raizen, and E.-L. Florin, *Direct Observation of the Full Transition from Ballistic to Diffusive Brownian Motion in a Liquid*, Nature Physics **7**, 576–580 (2011).

[103] A. P. Hammond and E. I. Corwin, *Direct measurement of the ballistic motion of a freely floating colloid in Newtonian and viscoelastic fluids*, Physical Review E **96**, 042606 (2017), publisher: American Physical Society.

[104] B. Lukić, S. Jeney, C. Tischer, A. J. Kulik, L. Forró, and E.-L. Florin, *Direct Observation of Nondiffusive Motion of a Brownian Particle*, Physical Review Letters **95**, 160601 (2005).

[105] T. Franosch, M. Grimm, M. Belushkin, F. M. Mor, G. Foffi, L. Forró, and S. Jeney, *Resonances Arising from Hydrodynamic Memory in Brownian Motion*, Nature **478**, 85–88 (2011).

[106] S. Kheifets, A. Simha, K. Melin, T. Li, and M. G. Raizen, *Observation of Brownian Motion in Liquids at Short Times: Instantaneous Velocity and Memory Loss*, Science **343**, 1493–1496 (2014).

[107] R. Zangi and L. J. Kaufman, *Frequency-Dependent Stokes-Einstein Relation in Supercooled Liquids*, Physical Review E **75**, 051501 (2007), publisher: American Physical Society.

[108] A. A. Chernov, *Replication of a Multicomponent Chain by the "Lightning" Mechanism*, Biophysics **12** (1967).

[109] D. E. Temkin, *One-Dimensional Random Walks in a Two-Component Chain*, Soviet Math. Docl. **13**, 1172–1176 (1972).

[110] S. Havlin and D. Ben-Avraham, *Diffusion in disordered media*, Advances in Physics **51**, 187–292 (2002), publisher: Taylor & Francis _eprint: https://doi.org/10.1080/00018730110116353.

[111] E. Bolthausen and A.-S. Sznitman, *Ten Lectures on Random Media* (Birkhäuser Basel, 2002).

[112] A.-S. Sznitman, *Topics in Random Walks in Random Environment*, Tech. Rep. 92-95003-25-X (International Atomic Energy Agency (IAEA), 2004).

[113] Z. Ofer, in *Lectures on Probability Thorey and Statistics, Lecture Notes*, Math, Vol. 1837 (Springer, Berlin, 2004) pp. 189–312.

[114] B. D. Hughes, *Random Walks and Random Environments: Random Walks* (Clarendon Press, 1995).

[115] H. Kesten, M. V. Kozlov, and F. Spitzer, *A limit law for random walk in a random environment*, Compositio Mathematica **30**, 145–168 (1975).

[116] Y. G. Sinai, *The Limiting Behavior of a One-Dimensional Random Walk in a Random Medium*, Theory of Probability & Its Applications **27**, 256–268 (1983), publisher: Society for Industrial and Applied Mathematics.

[117] J. P. Bouchaud, A. Comtet, A. Georges, and P. Le Doussal, *Classical Diffusion of a Particle in a One-Dimensional Random Force Field*, Annals of Physics **201**, 285–341 (1990).

[118] S. F. Burlatsky and J. M. Deutch, *Transient Relaxation of a Charged Polymer Chain Subject to an External Field in a Random Tube*, The Journal of Chemical Physics **109**, 2572–2578 (1998), publisher: American Institute of Physics.

[119] P. Le Doussal, C. Monthus, and D. S. Fisher, *Random Walkers in One-Dimensional Random Environments: Exact Renormalization Group Analysis*, Physical Review E **59**, 4795–4840 (1999), publisher: American Physical Society.

[120] L. F. Richardson and G. T. Walker, *Atmospheric Diffusion Shown on a Distance-Neighbour Graph*, Proceedings of the Royal Society of London. Series A, Containing Papers of a Mathematical and Physical Character **110**, 709–737 (1926), publisher: Royal Society.

[121] J. P. Bouchaud, *Diffusion and Localization of Waves in a Time-Varying Random Environment*, Europhysics Letters (EPL) **11**, 505–510 (1990), publisher: IOP Publishing.

[122] M. Chertkov and G. Falkovich, *Anomalous Scaling Exponents of a White-Advected Passive Scalar*, Physical Review Letters **76**, 2706–2709 (1996), publisher: American Physical Society.

[123] D. Bernard, K. Gawedzki, and A. Kupiainen, *Anomalous Scaling in the N-Point Functions of Passive Scalar*, Physical Review E **54**, 2564–2572 (1996), arXiv: chao-dyn/9601018.

[124] M.-C. Jullien, J. Paret, and P. Tabeling, *Richardson Pair Dispersion in Two-Dimensional Turbulence*, Physical Review Letters **82**, 2872–2875 (1999), publisher: American Physical Society.

[125] E. Balkovsky, G. Falkovich, and A. Fouxon, *Intermittent Distribution of Inertial Particles in Turbulent Flows*, Physical Review Letters **86**, 2790–2793 (2001), publisher: American Physical Society.

[126] F. Rassoul-Agha and T. Seppalainen, *An Almost Sure Invariance Principle for Random Walks in a Space-Time Random Environment*, Probability Theory and Related Fields **133**, 299–314 (2005), arXiv: math/0411602.

[127] J.-D. Deuschel, X. Guo, and A. F. Ramirez, *Quenched Invariance Principle for Random Walk in Time-Dependent Balanced Random Environment*, arXiv:1503.01964 [math] (2016), arXiv: 1503.01964.

[128] M. Balazs, F. Rassoul-Agha, and T. Seppalainen, *The Random Average Process and Random Walk in a Space-Time Random Environment in One Dimension*, Communications in Mathematical Physics **266**, 499–545 (2006), arXiv: math/0507226.

[129] I. Corwin, *The Kardar– Parisi– Zhang Equation and Universality Class*, Random Matrices: Theory and Applications **01**, 1130001 (2012), publisher: World Scientific Publishing Co.

[130] J. Quastel and H. Spohn, *The One-Dimensional KPZ Equation and Its Universality Class*, Journal of Statistical Physics **160**, 965–984 (2015).

[131] C. A. Tracy and H. Widom, *Level-Spacing Distributions and the Airy Kernel*, Physics Letters B **305**, 115–118 (1993).

[132] G. Barraquand and P. L. Doussal, *Moderate deviations for diffusion in time dependent random media*, Journal of Physics A: Mathematical and Theoretical **53**, 215002 (2020), publisher: IOP Publishing.

[133] M. Kardar, G. Parisi, and Y.-C. Zhang, *Dynamic Scaling of Growing Interfaces*, Physical Review Letters **56**, 889–892 (1986), publisher: American Physical Society.

[134] T. Sasamoto and H. Spohn, *One-Dimensional Kardar-Parisi-Zhang Equation: An Exact Solution and Its Universality*, Physical Review Letters **104**, 230602 (2010), publisher: American Physical Society.

[135] P. Calabrese, P. L. Doussal, and A. Rosso, *Free-Energy Distribution of the Directed Polymer at High Temperature*, EPL (Europhysics Letters) **90**, 20002 (2010), publisher: IOP Publishing.

[136] V. Dotsenko, *Bethe Ansatz Derivation of the Tracy-Widom Distribution for One-Dimensional Directed Polymers*, EPL (Europhysics Letters) **90**, 20003 (2010), publisher: IOP Publishing.

[137] G. Amir, I. Corwin, and J. Quastel, *Probability Distribution of the Free Energy of the Continuum Directed Random Polymer in 1+1 Dimensions*, Communications on Pure and Applied Mathematics **64**, 466–537 (2011), arXiv: 1003.0443.

[138] C. Sabot and L. Tournier, *Random Walks in Dirichlet Environment: An Overview*, Annales de la Faculté des sciences de Toulouse : Mathématiques **26**, 463–509 (2017).

[139] M. Balázs, F. Rassoul-Agha, and T. Seppäläinen, *Large Deviations and Wandering Exponent for Random Walk in a Dynamic Beta Environment*, The Annals of Probability **47**, 2186–2229 (2019), publisher: Institute of Mathematical Statistics.

[140] G. Barraquand and M. Rychnovsky, *Large Deviations for Sticky Brownian Motions*, Electronic Journal of Probability **25**, 1–52 (2020), publisher: Institute of Mathematical Statistics and Bernoulli Society.

[141] D. Brockington and J. Warren, *The Bethe Ansatz for Sticky Brownian Motions*, arXiv:2104.06482 [math] (2021), arXiv: 2104.06482.

[142] G. Oviedo, G. Panizo, and A. F. Ramírez, *Second Order Fluctuations of Large Deviations for Perturbed Random Walks*, arXiv:2108.02877 [math] (2021), arXiv: 2108.02877.

[143] S. Korotkikh, *Hidden Diagonal Integrability of Q-Hahn Vertex Model and Beta Polymer Model*, Probability Theory and Related Fields 10.1007/s00440-022-01117-0 (2022).

[144] A. Krajenbrink and P. L. Doussal, *The Crossover from the Macroscopic Fluctuation Theory to the Kardar-Parisi-Zhang Equation Controls the Large Deviations beyond Einstein's Diffusion*, arXiv:2204.04720 [cond-mat, physics:math-ph, physics:nlin] (2022), arXiv: 2204.04720.

[145] T. Alberts, K. Khanin, and J. Quastel, *Intermediate Disorder Regime for Directed Polymers in Dimension 1+1*, Physical Review Letters **105**, 090603 (2010), publisher: American Physical Society.

[146] J. Krug, P. Meakin, and T. Halpin-Healy, *Amplitude universality for driven interfaces and directed polymers in random media*, Phys. Rev. A **45**, 638–653 (1992), publisher: American Physical Society.

[147] S. Prolhac and H. Spohn, *The Height Distribution of the KPZ Equation with Sharp Wedge Initial Condition: Numerical Evaluations*, Physical Review E **84**, 011119 (2011), arXiv: 1105.0383.

[148] T. Halpin-Healy and K. A. Takeuchi, *A KPZ Cocktail-Shaken, Not Stirred...*, Journal of Statistical Physics **160**, 794–814 (2015).

[149] P. a. P. Moran, *Random Processes in Genetics*, Mathematical Proceedings of the Cambridge Philosophical Society **54**, 60–71 (1958), publisher: Cambridge University Press.

[150] W. G. Pollard and R. D. Present, *On Gaseous Self-Diffusion in Long Capillary Tubes*, Physical Review **73**, 762–774 (1948), publisher: American Physical Society.

[151] S. Ahmadi and R. K. Bowles, *Diffusion in quasi-one-dimensional channels: A small system n, p, T, transition state theory for hopping times*, The Journal of Chemical Physics **146**, 154505 (2017), publisher: American Institute of Physics.

[152] M. Prähofer and H. Spohn, *Universal Distributions for Growth Processes in 1+1 Dimensions and Random Matrices*, Physical Review Letters **84**, 4882–4885 (2000), publisher: American Physical Society.

[153] A. V. Chechkin, F. Seno, R. Metzler, and I. M. Sokolov, *Brownian yet Non-Gaussian Diffusion: From Superstatistics to Subordination of Diffusing Diffusivities*, Phys. Rev. X **7**, 021002 (2017), publisher: American Physical Society.

[154] S. H. Noskowicz and I. Goldhirsch, *Average versus Typical Mean First-Passage Time in a Random Random Walk*, Physical Review Letters **61**, 500–502 (1988), publisher: American Physical Society.

[155] P. Le Doussal, *First-passage time for random walks in random environments*, Phys. Rev. Lett. **62**, 3097–3097 (1989), publisher: American Physical Society.

[156] Y. Zhang and O. K. Dudko, *First-Passage Processes in the Genome*, Annual Review of Biophysics **45**, 117–134 (2016).

[157] J. B. Hass, H. Drillick, I. Corwin, and E. I. Corwin, *Extreme Diffusion Measures Statistical Fluctuations of the Environment*, Physical Review Letters **133**, 267102 (2024), publisher: American Physical Society.

[158] R. Parthasarathy, *Rapid, accurate particle tracking by calculation of radial symmetry centers*, Nature Methods **9**, 724–726 (2012), publisher: Nature Publishing Group.

[159] A. Ishimaru, *Diffusion of light in turbid material*, Applied Optics **28**, 2210–2215 (1989), publisher: Optica Publishing Group.

[160] C. F. Bohren and D. R. Huffman, *Absorption and Scattering of Light by Small Particles* (Wiley, 1983).

[161] K. M. Yoo and R. R. Alfano, *Time-resolved coherent and incoherent components of forward light scattering in random media*, Optics Letters **15**, 320–322 (1990), publisher: Optica Publishing Group.

[162] O. K. Dudko and G. H. Weiss, *Photon diffusion in biological tissues*, Diffusion Fundamentals **2**, 10.62721/diffusion-fundamentals.2.300 (2005).

[163] S. I. Heizler, *The Asymptotic Telegrapher's Equation (P1) Approximation for Time-Dependent, Thermal Radiative Transfer*, Transport Theory and Statistical Physics **41**, 175–199 (2012), publisher: Taylor and Francis.

[164] B. J. Hoenders and R. Graaff, *Telegrapher's equation for light derived from the transport equation*, Optics Communications **255**, 184–195 (2005).

[165] G. H. Weiss, *Some applications of persistent random walks and the telegrapher's equation*, Physica A: Statistical Mechanics and its Applications **311**, 381–410 (2002).

[166] A. Godec and R. Metzler, *First passage time distribution in heterogeneity controlled kinetics: going beyond the mean first passage time*, Scientific Reports **6**, 20349 (2016), number: 1 Publisher: Nature Publishing Group.

[167] H.-M. Chun, S. Hwang, B. Kahng, H. Rieger, and J. D. Noh, *Heterogeneous Mean First-Passage Time Scaling in Fractal Media*, Physical Review Letters **131**, 227101 (2023), publisher: American Physical Society.

[168] G. Zsurkis, J. Nicolau, and P. M. M. Rodrigues, *First passage times in portfolio optimization: A novel nonparametric approach*, European Journal of Operational Research **312**, 1074–1085 (2024).

[169] Z. Schuss, K. Basnayake, and D. Holcman, *Redundancy principle and the role of extreme statistics in molecular and cellular biology*, Physics of Life Reviews **28**, 52–79 (2019).

[170] B. Meerson and S. Redner, *Mortality, Redundancy, and Diversity in Stochastic Search*, Physical Review Letters **114**, 198101 (2015), publisher: American Physical Society.

[171] C. J. Lee, P. J. M. v. d. Slot, and K.-J. Boller, *Using ultra-short pulses to determine particle size and density distributions*, Optics Express **15**, 12483–12497 (2007), publisher: Optica Publishing Group.

[172] S. J. Madsen, B. C. Wilson, M. S. Patterson, Y. D. Park, S. L. Jacques, and Y. Hefetz, *Experimental tests of a simple diffusion model for the estimation of scattering and absorption coefficients of turbid media from time-resolved diffuse reflectance measurements*, Applied Optics **31**, 3509–3517 (1992), publisher: Optica Publishing Group.

[173] A. Ishimaru, *Diffusion of a pulse in densely distributed scatterers*, JOSA **68**, 1045–1050 (1978), publisher: Optica Publishing Group.

[174] C. Calba, L. Méès, C. Rozé, and T. Girasole, *Ultrashort pulse propagation through a strongly scattering medium: simulation and experiments*, JOSA A **25**, 1541–1550 (2008), publisher: Optica Publishing Group.

[175] V. Rossetto, *Isotropic radiative transfer as a phase space process: Lorentz covariant Green's functions and first-passage times*, Europhysics Letters **139**, 11001 (2022), publisher: EDP Sciences, IOP Publishing and Società Italiana di Fisica.

[176] W. F. Long and D. H. Burns, *Particle sizing and optical constant measurement in granular samples using statistical descriptors of photon time-of-flight distributions*, Analytica Chimica Acta **434**, 113–123 (2001).

[177] C. Zeller and R. Cordery, *Light scattering as a Poisson process and first-passage probability*, Journal of Statistical Mechanics: Theory and Experiment **2020**, 063404 (2020), publisher: IOP Publishing and SISSA.

[178] G. Deželić and J. P. Kratohvil, *Determination of size of small particles by light scattering. experiments on ludox colloidal silica*, Kolloid-Zeitschrift **173**, 38–48 (1960).

[179] B. E. Bonnelycke and W. B. Dandliker, *Light scattering of colloidal silica*, Journal of Colloid Science **14**, 567–571 (1959).

[180] D. A. I. Goring, M. Senez, B. Melanson, and M. M. Huque, *Light-scattering calibration with Ludox*, Journal of Colloid Science **12**, 412–416 (1957).

[181] J. R. Lakowicz, ed., *Principles of Fluorescence Spectroscopy* (Springer US, Boston, MA, 2006).

[182] T. I. Gombosi, J. R. Jokipii, J. Kota, K. Lorencz, and L. L. Williams, *The Telegraph Equation in Charged Particle Transport*, The Astrophysical Journal **403**, 377 (1993), publisher: IOP.

[183] A. Schuster, *Radiation Through a Foggy Atmosphere*, The Astrophysical Journal **21**, 1 (1905), publisher: IOP.

[184] G. H. Weiss, *First passage times for correlated random walks and some generalizations*, Journal of Statistical Physics **37**, 325–330 (1984).

[185] J. Masoliver, J. M. Porrà, and G. H. Weiss, *Solution to the telegrapher's equation in the presence of reflecting and partly reflecting boundaries*, Physical Review E **48**, 939–944 (1993), publisher: American Physical Society.

[186] J. Masoliver and G. H. Weiss, *Telegrapher's equations with variable propagation speeds*, Physical Review E **49**, 3852–3854 (1994), publisher: American Physical Society.

[187] L. Pattelli, A. Egel, U. Lemmer, and D. S. Wiersma, *Role of packing density and spatial correlations in strongly scattering 3D systems*, Optica **5**, 1037–1045 (2018), publisher: Optica Publishing Group.

[188] L. Pattelli and G. Mazzamuto, *Experimental imaging and Monte Carlo modeling of ultrafast pulse propagation in thin scattering slabs*, Journal of Biomedical Optics **27**, 083020 (2022), publisher: SPIE.

[189] E. Pini, G. Mazzamuto, F. Riboli, D. S. Wiersma, and L. Pattelli, *Non-self-similar light transport in scattering media*, Physical Review Research **6**, L032026 (2024), publisher: American Physical Society.

[190] R. Rezvani Naraghi, S. Sukhov, J. Sáenz, and A. Dogariu, *Near-Field Effects in Mesoscopic Light Transport*, Physical Review Letters **115**, 203903 (2015), publisher: American Physical Society.